NOVA SCHOOL OF SCIENCE & TECHNOLOGY

DEPARTMENT OF ELECTRICAL AND COMPUTER ENGINEERING

JOÃO PEDRO SECO RAMOS VIEIRA FERREIRA

BSc in Electrical Engineering

PHYSICAL LAYER SECURITY OF LARGE ANTENNA ARRAYS OPERATING IN THE NEAR-FIELD

NEAR-FIELD BEAMFOCUSING AND THE STUDY OF IT'S PHYSICAL LAYER SECURITY CAPABILITIES

MASTER IN ELECTRICAL AND COMPUTER ENGINEERING

NOVA University Lisbon
July, 2023

NOVA SCHOOL OF SCIENCE & TECHNOLOGY

DEPARTMENT OF ELECTRICAL AND COMPUTER ENGINEERING

PHYSICAL LAYER SECURITY OF LARGE ANTENNA ARRAYS OPERATING IN THE NEAR-FIELD

NEAR-FIELD BEAMFOCUSING AND THE STUDY OF IT'S PHYSICAL LAYER SECURITY CAPABILITIES

JOÃO PEDRO SECO RAMOS VIEIRA FERREIRA

BSc in Electrical Engineering

Advisers: João Francisco Martinho Lêdo Guerreiro
Assistant Professor, NOVA University Lisbon
Rui Dinis
Full Professor, NOVA University Lisbon

Examination Committee

Chairs: Paulo Miguel de Araújo Borges Montezuma de Carvalho
Associate Professor, NOVA University Lisbon
Nuno Filipe Silva Veríssimo Paulino
Associate Professor with aggregation, NOVA University Lisbon

Adviser: João Francisco Martinho Lêdo Guerreiro
Assistant Professor, NOVA University Lisbon

MASTER IN ELECTRICAL AND COMPUTER ENGINEERING
SPECIALIZATION IN TELECOMMUNICATIONS

NOVA University Lisbon
July, 2023

Acknowledgements

I would like to extend my gratitude to the advisers who have guided me throughout the completion of this thesis. I want to thank Professor Rui Dinis for serving as my adviser. A special and warm thanks go to Professor João Guerreiro, whose unwavering assistance and dedication have been invaluable. Throughout this journey, Professor Guerreiro consistently went above and beyond to provide me with the best possible support and guidance. Your expertise and commitment have truly made a significant impact on the quality and success of this thesis.

I would like to express my heartfelt gratitude to FCT NOVA, the university that has been my academic home for the past five years. Throughout this time, FCT NOVA has provided me with an exceptional environment for learning, growth, and exploration. The dedicated faculty, staff, and fellow students have shaped my academic journey, offered support and inspired me to reach new heights.

In my academic journey, I have been fortunate to have a support system that has guided me through the ups and downs. It's like walking along a path where my dad and Tiago, with their unwavering determination and wisdom, walk ahead of me, inspiring me to keep pushing forward and strive for excellence. Their footsteps serve as a constant reminder of the possibilities and successes that lie ahead. Simultaneously, my mom and my sister walk behind me, providing the much-needed support and encouragement to help me rise again whenever I stumble or face challenges along the way. They lend a helping hand, offering comfort, guidance, and the belief that I am capable of overcoming any obstacles that come my way.

The boys from Gang Farm, Futawrld, and the Ranjews also deserve a shout-out. Together, we navigate the twists and turns of life, sharing experiences, exchanging ideas, and celebrating each other's achievements. Their presence brings joy, warmth, and a sense of community, reminding me that I am never alone in this pursuit.

Last but not least, I would also like to thank Ritinha for always being there for me. Thank you for growing up with me and letting me unravel life's stages by your side. You are my partner in crime, if crime was spending the whole day listening to music you don't like while cuddling.

Abstract

This thesis explores the security aspects of near-field communications in the context of the upcoming 6th Generation wireless technology. With each decade witnessing significant advancements in cellular wireless communications, the demand for faster, more accessible, and secure networks continues to grow. Traditional security approaches relying on higher-layer cryptography techniques may not be sufficient for the future massively connected world. Therefore, this research focuses on leveraging physical layer security techniques, specifically in the near-field regime, to enhance the confidentiality and privacy of wireless communications.

The study begins with an examination of the state of the art, encompassing previous telecommunication generations, Multiple-Input Multiple-Output systems, Multiple-Input Multiple-Output with Extremely Large Antenna Arrays, and an overview of physical layer security concepts. Subsequently, a comprehensive analysis of the near-field channel modeling components is presented, exploring the unique propagation characteristics of electromagnetic waves within this region.

The thesis then delves into the exploration of physical layer security at the near-field, employing the established channel model to calculate the secrecy rate in the downlink and achievable capacity in the uplink. Various scenarios involving a malicious user in the communication link are considered, highlighting the inherent security capabilities of near-field communications.

In conclusion, this research contributes to the advancement of secure communication technologies by providing insights into the physical layer security aspects of near-field communications in the context of 6th Generation. The findings show the potential of utilizing the propagation features of large antenna arrays such as the limited-depth beamforming to enhance security and privacy. The practical implications and potential applications of the research outcomes are also discussed.

Keywords: Wireless communications, 6G, Physical layer security, Near-field communications, Channel modeling, Beamforming, Extremely Large Antenna Arrays, Secrecy rate, Achievable capacity

Resumo

Esta tese explora os aspetos de segurança das comunicações de campo próximo no contexto da próxima tecnologia sem fios 6G. A cada década, testemunhamos avanços significativos nas comunicações sem fio, a demanda por redes mais rápidas, acessíveis e seguras continua a crescer. Abordagens tradicionais de segurança que dependem de técnicas criptográficas em camadas superiores podem não ser suficientes para o futuro mundo altamente conectado. Portanto, esta pesquisa concentra-se nas técnicas de seguraça a nivél físico, especificamente no regime de campo próximo, para melhorar a confidencialidade e privacidade das comunicações sem fio.

O estudo começa com uma análise do estado da arte, abrangendo gerações anteriores de telecomunicações, sistemas Multiple Input Multiple Output (MIMO), MIMO com Extremely Large Antenna Arrays (ELAA)s, e uma visão geral dos conceitos de seguraça a nivél físico. Posteriormente, é apresentada uma análise abrangente dos componentes de modelagem do canal no campo próximo, explorando as características únicas de propagação de ondas eletromagnéticas nesta região.

A tese, em seguida, aprofunda a exploração de seguraça a nivél físico no campo próximo, empregando o modelo de canal estabelecido para calcular a "Secrecy Rate"no "Downlink"e a capacidade máxima atingivel no "Uplink". Vários cenários envolvendo um utilizador malicioso na ligação de comunicação são considerados, destacando as capacidades inerentes de segurança das comunicações no campo próximo.

Em conclusão, esta pesquisa contribui para o avanço das tecnologias de comunicação segura, fornecendo informações sobre os aspetos de segurança da camada física das comunicações no campo próximo no contexto de 6G. Os resultados mostram o potencial de utilizar as características de propagação de grandes matrizes de antenas, como o feixe de profundidade limitada, para melhorar a segurança e a privacidade. As implicações práticas e potenciais

aplicações dos resultados da pesquisa também são discutidas.

Palavras-chave: Comunicações sem fios, 6G, Segurança a Nivel Físico, Comunicações no Campo Próximo, Modelo de Canal, Beamforming, Extremely Large Antenna Arrays, Secrecy rate, Capacidade

Contents

List of Figures

Acronyms

1G	1st Generation
5G	5th Generation
6G	6th Generation
AI	Artificial Intelligence
AoA	Angle-of-Arrival
AWGN	Additive White Gaussian Noise
BS	Base Station
CIR	Channel Impulse Response
CSI	Channel State Information
DF	Depth-of-Focus
DoF	Degrees of Freedom
DoS	Denial of Service
DSSS	Direct Sequence Spread Spectrum
ELAA	Extremely Large Antenna Arrays
eMBB	Enhanced Mobile Broadband
FDD	Frequency Division Duplexing
FHSS	Frequency Hopping Spread Spectrum
GPS	Global Positioning System
HARQ	Hybrid Automatic Repeat Request
IBI	Inter-Band Interference

IoE	Internet of Everything
IoT	Internet of Things
ISI	Inter-Symbol Interference
LAA	Large Antenna Arrays
LIS	Large Intelligent Surfaces
LMMSE	Linear Minimum Mean Squared Error
LoS	Line of Sight
LS	Least Squares
MAC	Media Access Control
MBUST	Multi-Band Ultrafast-Speed Transmission
MD-IM	Multi-Domain Index Modulation
MDJT	Multi-Domain Joint Transmission
MF	Matched Filtering
MIMO	Multiple Input Multiple Output
MISO	Multiple Input Single Output
ML	Machine Learning
mMIMO	massive Multi-Input Multi-Output
mMTC	Massive Machine-Type Communications
mmWave	millimeter-wave
MSE	Mean Squared Error
OAM-MDM	Orbital Angular Momentum-Based Mode-Division Multiplexing
OSI	Open Systems Interconnection
PLS	Physical Layer Security
QoS	Quality of Service
RF	Radio Frequency
RFID	Radio Frequency Identification
RIS	Reconfigurable Intelligent Surfaces
RTT	Round Trip Time
SDMA	Space Division Multiple Access
SDN	Software Defined Networking
SDR	Software Defined Radio
SFIN	Super Flexible Integrated Network

SIMO	Single Input Multiple Output
SISO	Single Input Single Output
SNJR	signal-to-noise plus jamming ratio
SNR	signal-to-noise ratio
SVD	Singular Value Decomposition
TDD	Time Division Duplexing
TTI	Transmission Time Intervals
UE	User Equipment
UHD	Ultra High Definition
ULA	Uniform Linear Arrays
URLLC	Ultra-Reliable and Low-Latency Communications

Symbols

A	Area of an antenna element
A_{ELAA}	Area of the array
α	Occupation Ratio
C	Capacity
c	Light speed in a vacuum
D	Diagonal of an antenna element
d	Distance between transmitter and center of the element
d'	Distance between transmitter and edge of the element
d_x	Displacement
D_{ELAA}	Diagonal of the array
d_{FA}	Fraunhofer array distance
d_F	Fraunhofer distance
ϵ	Permittivity of free space
f_c	Carrier frequency
$\boldsymbol{I}$	Identity matrix
j	Imaginary unit
k	Wave number
L	Length of the side of an antenna element
λ	Wavelength
μ	Permeability of free space

N	Number of antenna elements
N_{Op}	Number of active antenna elements
∇	Nabla operator
ω	Angular frequency
P_N	Noise power
P_T	Transmitted power
ρ	Signal to noise ratio
S	Secrecy rate
Z_0	Free space impedance

1 Introduction

1.1 Context

In a dynamic and demanding society, technology must adapt and evolve to fit its needs. Since the early seventies, a leap in the development of cellular wireless communications has been observed every decade. As the world becomes increasingly connected, demand for more speed, accessibility, availability, and lower latency is required of radio network infrastructures. Besides these great advancements in wireless communications in the last years, there has been an increased interest in secure communications and this has become crucial for the next generation of wireless communications.

After the commercial deployment of the 5th Generation (5G), the 6th Generation (6G) follows and engineers have still a long way to go in the research and development of this technology. With this, also comes the security aspects of the wireless system. Although higher layers of the Open Systems Interconnection (OSI) model are usually responsible for some of the communication's security, the physical layer can also provide some interesting and creative solutions to increase the secrecy and the resilience to jamming attacks. In this work, the Physical Layer Security (PLS) features of the novel near field communications being proposed for 6G will be analyzed. This includes the derivation of the channel model valid for this propagation region as well as the investigation of different communication scenarios from a security perspective.

1.2 Motivation & Objectives

The newly developed massive connectivity of the modern world makes confidentiality uniquely important. The ever-growing demand for general accessibility and quality of use of telecommunications systems needs to be paired with a security and privacy paradigm strong enough to account for its demands.

Traditional approaches rely on higher-layer cryptography techniques, and although advanced and robust, they might not suffice for the massively connected future ahead. Pairing with such techniques, PLS can be used for secure key exchange in encryption as

this type of layer security uses the physical properties of the channel, like fading and interference to enhance the signal strength of the legitimate user whilst lowering the malicious users' channel quality in the case of eavesdropping.

Moreover, keyless solutions are being studied, these solutions avoid the algorithmic complexities of secret key distribution and management and offer a competitive aspect in this regard. Since it is envisioned that 6G will be based on ELAAs as well as on large carrier frequencies, it is likely that communications might not occur in the far field as is commonly assumed in current wireless communications systems, but rather occur in the radiative near field region.

In light of this communication type, a different approach to channel modeling and beamforming is required to fully exploit its benefits and explore its intrinsic PLS features. The main objective is to study the physical layer security capabilities of a large antenna array operating in the near field. This involves:

- Deriving and implementing a channel model for an ELAA.
- Characterizing the array gain and beamforming capabilities.
- Analyzing the PLS aspects of near field beamforming.

The research aims to enhance understanding and contribute to the advancement of secure communication technologies.

1.3 Overview

The subsequent sections of this document adhere to the following structure. Section 2 encompasses a comprehensive examination of the "State of The Art" and serves as a summary of the literature review. The topics covered in this section include an exploration of previous telecommunication generations, a detailed analysis of general concepts related to MIMO systems, an examination of MIMO with ELAA, and, finally, a subsection dedicated to PLS.

The subsequent section 3 offers a comprehensive analysis of the channel modeling components pertaining to the near field regime. It encompasses a meticulous analysis of the propagation characteristics associated with electromagnetic waves propagated within this region. Furthermore, a correlation is established with the Friis formulas specifically within the context of the far field region.

Subsequently, section 4 delves into a comprehensive exploration of various subjects related to security at the physical layer of the OSI stack. This section leverages the established channel model to conduct calculations encompassing secrecy rate and achievable capacity. The objective is to showcase the inherent PLS capabilities in near field communication, given a malicious element in the communication.

The last section concludes this thesis by summarizing the key findings and contributions of the research conducted. It summarizes the main objectives, the methodologies

employed, and results obtained throughout the study. Additionally, the section offers insights into the practical implications and potential applications of the research outcomes.

1.4 Publications

From the work developed in this thesis, the following conference article has been published: "J. Ferreira, J. Guerreiro, R. Dinis, M. Silva, "On the Jamming Rejection Features of Near Field Beamforming," IEEE VTC 2023 (Spring), Florence, Italy, June 2023.

2

State of The Art

This section provides the reader with an understanding of the natural progression of the state-of-the-art, namely a background on the relevant telecommunication generations, as well as an introduction to the basics of MIMO, ELAA and concepts of PLS.

After the historical context is given in section 2.1, the reader will have gathered sufficient knowledge to apprehend what is to be discussed in the following sections 2.2, namely, the parallels that will be established between the technologies of massive Multi-Input Multi-Output (mMIMO) Beam-forming in the 5th generation of mobile telecommunications and Beam-focusing with ELAA in the next generations, as well as a thorough description of the benefits and challenges that have risen with this emerging technologies.

To present a comprehensive discussion on the subject matter, this literature review will also touch on how, recently, we have seen a growing research effort on wireless communications using ELAA, namely Reconfigurable Intelligent Surfaces (RIS) and Large Intelligent Surfaces (LIS) in section 2.3, and how they have been used to conceive new wireless transceiver architectures, stepping into the supposed new generations.

Channel modeling and beam-forming will also be discussed. Then, in the final subsection 2.4, we will tackle another major subject matter, the PLS. It will be described how one can manipulate the characteristics of these emerging technologies to exploit the intrinsic physical security characteristics of near-field communications. This subsection of the literature review is of paramount importance for comprehending the inherent distinctions associated with operating in the near-field and far-field regions of an antenna. It also aims to address the question: "How can we leverage the physical characteristics of the channel to effectively communicate information and protect it against malicious users?". The answer to this question represents a primary objective of the present thesis.

2.1 5G and Beyond

In this subsection of the state of the art, it is presented the 5^{th} generation of mobile communications, being discussed its relevance as the main driver behind the creation of an interconnected society. Different topics will be analyzed regarding this telecommunication

generation such as its inherent solutions for vertical markets, requirements and different application scenarios and flexibility.

After going through the related work regarding 5G, we shall set our sights beyond the current paradigm and start to envision the next generation yet to come, the 6th generation of mobile communications. We will go over the main aspects it might bring to the table, the central technologies for its development and future deployment, as well as the major characteristics of the newfound near-field communications, such as its fundamentals, the challenges currently identified, and the future directions that this technology might take.

2.1.1 5th Generation

Roughly every ten years we expect a new mobile access technology to hit the consumer market. This phenomenon has been occurring since the early 1980s with the appearance of the first generation of cellular analog communication systems, i.e., the so-called 1st Generation (1G) [1].

The increasing number of subscribers to the mobile network system gave rise to the demand for more connectivity, faster internet access, and low-latency communications. These factors have been dictating the evolution of wireless communications and, in fact, have been the main drivers for the research and development of new, improved telecommunications networks [2].

Despite the extreme increase in capacity demand over the last decade, the applications of 5G are not just limited to accommodating the mobile broadband network. In fact, the 5th generation of telecommunications networks has many applications that can be divided into three main use cases, schematically depicted in figure 2.1.1 namely:

- Massive Machine-Type Communications.
- Ultra-Reliable and Low-Latency Communications.
- Enhanced Mobile Broadband.

Although older telecommunication generations were more focused on increasing spectral efficiency and mobile broadband, it can be observed that the new generation was also driven by a number of newly emerging use cases. Among them, the Massive Machine-Type Communications (mMTC). Massive Machine-Type Communications are about wireless connectivity and have some strict requirements, such as 1 million connections per km^2, a high degree of coverage even in indoor scenarios, as well as low power consumption for increased battery lifetimes, with targets of at least 10 years [3].

Ultra-Reliable and Low-Latency Communications (URLLC) is another use case of 5G that is dedicated to accommodating new applications that involve rigorous reliability and latency requirements. Despite the other two categories of 5G use cases mentioned above, URLLCis considered to be the one with the most demanding requirements: low latency and ultra-high reliability [4]. Technological pillars and solutions for lower latency were the use of shorter Transmission Time Intervals (TTI), preemptive scheduling and

self-contained subframes as well as shorter Hybrid Automatic Repeat Request (HARQ) Round Trip Time (RTT). By trading big packet sizes and overall channel throughput we can come to a compromise and get smaller packet sizes, ultra-reliability and low latency can be achievable [5].

Despite 5G's early parameter standardization stage, some include 10 Gbps peak data rate with 100 Mbps at the cell edge, a significant step up in comparison with earlier generations. Some requirements for Enhanced Mobile Broadband (eMBB) are a wider range of code rates, length, and modulation order. In order to commit to these requirements, 5G will need to prompt significant advancements regarding spectral and signaling efficiency as well as bandwidth when compared to previous generations [6]. The key enablers for this technology are the extreme densification of urban areas, the usage of novel communication techniques such as mMIMO, which will be detailed later in this section, and the usage of millimeter-wave (mmWave) spectrum [7]. Thus, 5G provisions a solid foundation and is seen as an inherent solution for vertical markets. Vertical markets, which are ventured by these new advancements regarding enhanced capacity, ultra-high reliability, and massive connectivity, are industries highly focused on a specific niche market, such as:

- eHealth.
- Factory of the future.
- Automotive.
- Media & Entertainment.

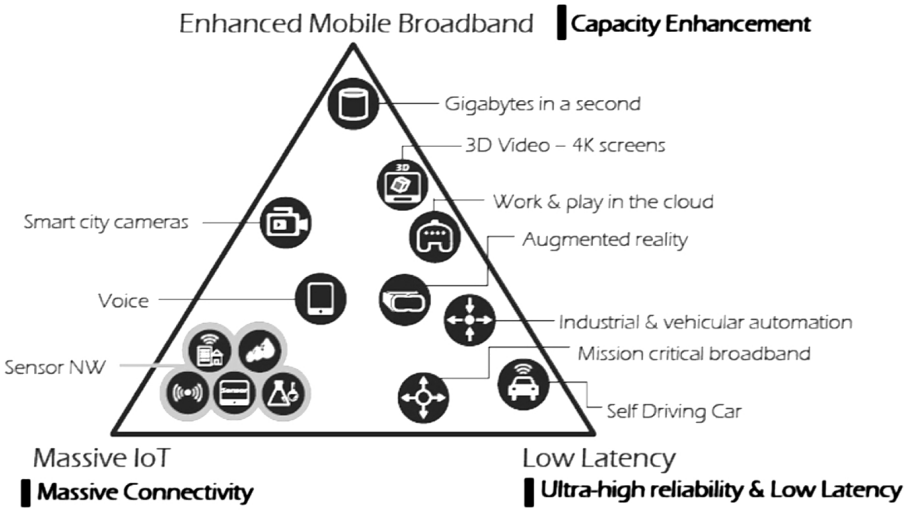

Figure 2.1: 5G use cases and its key performance requirements [8].

A vision on 5G access infrastructure: Large Antenna Arrays (LAA) are envisioned for 5G communications systems, as to cope with mmWave spectrum we will need many antennas to guarantee the minimum Quality of Service Quality of Service (QoS) levels [9]. Also, the number of antennas in the Base Station (BS) will be much larger than the ones

found in the User Equipment (UE), for practicality as well as energy consumption reasons and efficiency criteria [10].

With the increase of the number of elements in the antenna arrays, these LAA might start to take shapes such as linear, rectangular, and in some cases circular - Uniform Linear Arrays (ULA) being the most common so far [11]. The relative size of the arrays might depend on the spacing between elements, as for the spatial resolution of users in 3D space they need to be half a wavelength ($\lambda/2$) apart, thus depending only on the operation frequency of the array. Moreover, beamforming structures, power amplifiers, and phase shifters should be packed behind the antenna element.

In 5G we have the capability of spatial diversity and multiplexing to improve the system's robustness when dealing with frequency selective fading channels and for improving the general capacity by utilizing different paths to carry additional information. These topics will be further analyzed in section 2.2.1.

2.1.2 6th Generation

With the advancements of 5G technologies, some countries and organizations around the world have made have been partnering on the research of the preliminary vision and supporting techniques for 6G wireless mobile networks. When it comes to the physical layer, the main techniques being proposed to support 6G are: advanced forward error correction coding, new channel modulation techniques, and new antenna systems [12]. Like the current generation of telecommunication systems, 6G will also present requirements corresponding to natural drivers pushed by our conception of the interconnected society we might inhabit in around 10 years.

To accommodate the progress expected of the 4^{th} industrial revolution, the next generation must present:

- Super Flexible Integrated Network.
- Multi-Mode & Multi-Domain Joint Transmission.
- Machine Learning and Big Data Assisted Intelligent Transmission.
- Multi-Band Ultrafast-Speed Transmission.

We can look at Super Flexible Integrated Network (SFIN) as an upgrade of the well-known 5G's mMTC. 6G will serve as a door to many futuristic scenarios, such as the rise of smart homes and smart cities - Not only it will be expected to fulfill the previous generations' endeavor to provide mMTC but also human-to-machine type communications. The prospect is to evolve from a paradigm of the Internet of Things (IoT) to one more accurately described by the Internet of Everything (IoE). This integration will require mass densification of the network and integration of terrestrial, aerial networks, and satellite systems. Some studies are proposing solutions to this integration, like in [13], where a Media Access Control (MAC) protocol is presented to integrate THz-Based heterogeneous networks, and in [14], where an architecture is also proposed.

One of the biggest problems for future generations will be the physical medium techniques by which data will be processed and transmitted. The ability to cope with molecular absorption and spreading loss due to such high frequencies is one of the main focal points in research, [15]. This is why we shall adopt a distance-adaptive physical layer design together with Multi-Domain Joint Transmission (MDJT) techniques. In [15], the authors have analyzed the current state of the art when it comes to combating the distance problem at mmWave to THz frequencies, regarding the physical layer design aspect.

A distance adaptive design should take into account the available channel bandwidth defined by the propagation media molecular absorption. In their work, [16] Han et al. derived a framework to extract the waveform to maximize effective communication distance[1] at a constant capacity and transmit power by taking into account Inter-Symbol Interference (ISI) and Inter-Band Interference (IBI). Again in [17], Han et al. developed an allocation scheme that takes into account modulation, spectrum, and transmit power. Here, they found that we can achieve increased communication distance at the expense of hardware complexity [17]. Multi-domain joint transmission models such as Orbital Angular Momentum-Based Mode-Division Multiplexing (OAM-MDM) [17] and Multi-Domain Index Modulation (MD-IM) [18] can also be employed to enhance data transmission.

Machine Learning (ML) and Artificial Intelligence (AI) based approaches are thought to be key in the field of channel estimation, synchronization, equalization, and channel detection in 6G. In a paradigm of extremely low latency, tediously long calculations can be bypassed by using such methods. In the forethought, massively connected and heterogeneous future, ML and big data analysis are thought to work together to enhance mobile networks predictability and self-adaption [19].

The current evolution rate of modern society suggests that the current frequency band might not suffice the growing capacity demand. In an example given in [20], an uncompressed Ultra High Definition (UHD) (4K and 8K) video may reach 24 Gb/s, and some 3D renderizations may reach to 100 Gb/s - These types of data transfers are expected to become more common in a not so distant future. Thus we are looking forward to reaching wireless technologies that go beyond 5G's mmWave spectrum and tap into unexplored terahertz bands to combat future spectrum paucity and still be able to provide user bandwidth from 100 MHz to 1 THz [12].

Multi-Band Ultrafast-Speed Transmission (MBUST) will rely not only on the exploration of this frequency band but also on the dynamic use of multiple different frequencies in this new range with the help of advanced Software Defined Radio (SDR) and Software Defined Networking (SDN) techniques [12].

Like in 5G, the prospect of the realization of some of these aspects allows us to speculate about our future society and the future directions of the industry. Most of the use cases explored next will be in some way expansions of the ones discussed previously in 5G. Only when the new 6G enablers become available, more possible cases might emerge.

[1] Since THz frequency communication naturally enables extremely high data rates, the constraint becomes the distance of communication.

While in 5G we were trying to break the communication barrier, here we are pushing the limits of physical communication:

- Enhanced Virtual Reality.
- Integrated Ultra Smart City.
- New Communications Terminals.

In the field of Enhanced Virtual Reality, we are mainly talking about accurate indoor positioning, holographic communication, and the development of ultra-sensitive haptic feedback technology. Holographic communications may become the natural next step progression of communication technology. In a world where voice calls and video streaming may not suffice, the realistic projection of a 3D object through the ether with minimal delay may become the solution. A type of communication where one can interact with the holographic data in real-time will require an extremely large amount of bandwidth [21]. Parallel to holographic communication, we have the emerging technology of tactile communication with the development of haptic feedback. With the help of this technology we could remotely exchange physical interaction itself in real-time [22] - Yet this technology may still be in its early stages due to complications over packet size and reliability which may still be a long way to come [23]. Due to the rich propagation environment associated with an indoor setting, Global Positioning System (GPS), may still be a long way until we become able to accurately position inside a building, despite novel triangulation techniques using Wi-fi signal strength are getting some traction [24].

The integrated ultra smart city paradigm introduces the evolution of the concept of a Smart city, a city where its citizens' quality of life is enhanced by automation and interconnection of city infrastructure, such as public transportation and ubiquitous self-driving vehicular modules [25]. To draw another parallel between 5G and 6G, in the previous generation - 5G's smart cities are already thought to have independent smart utilities, like electricity, water, and garbage collection, however, 6G will take this a step further and approach this holistically. We have examples of a "Super Smart Home Environment" [26], where house appliances and utilities will be interconnected and the user may be able to interact with them by using only voice or gestures, kickstarting a paradigm shift in the design of future housing. The integration of healthcare in this discussion must also be paramount, as we progress in society and the average life span increases, a new problem arises, the growing aging population. A step up from 5G's eHealth, with the help of new technologies such as haptic feedback, holographic communications, and state-of-the-art URLLC we could have access to remote surgery from the most qualified doctors from everywhere in the world, and increase human interaction by allowing elders to be closer to their relatives with enhanced virtual reality [25].

With the growing technological advancements regarding peripheral devices and the increasing number of communication accessories, we should expect the emergence of integrated headsets or even implanted devices [27]. This largely covers the new communications terminals section. Energy efficiency, reliability, and security will be the main

pushing forces for this emerging technology. Some small-scale applications of such devices are already available like small Radio Frequency Identification (RFID) chip implants. Other companies like Neuralink are trying to map thought in the human brain, another step into this paradigm [25].

Some work has been done in the field of what is to become the foundation of beyond 5G radio access networks. The idea that users are always located in the far field no longer holds for the high-frequency bands and extremely high bandwidth characterized by the 6G communication paradigm. Hence, communication is expected to occur in the radiating near-field. In order to support such ambitious metrics, LIS together with RIS, are expected to be deployed in a densely packed manner in urban areas, in order to cope with the range and energy demands of this new sub-THz band equipment, a depiction of this scenario is shown in figure 2.1.2. The fact that we will mostly operate in the near field, will result in some intrinsic physical characteristics of the signal that we shall exploit to our advantage. The round wavefront resulting from the near-field communication realizes the possibility of beam-focusing, an analogous technique to the well-known and used beam-forming in current communication wireless technologies [28].

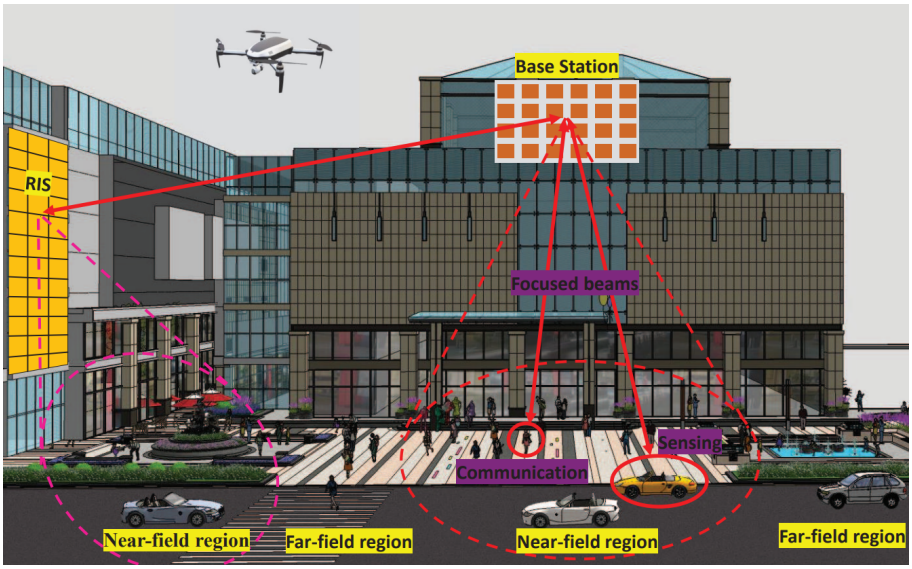

Figure 2.2: Example scenario of ELAA and RIS aided communication in the near-field [28]

2.2 Conventional MIMO Systems

As previously stated, MIMO stands for Multi-Input Multi-Output. The different types of MIMO configurations are derived based on the number of transmit and receive antennas. Essentially, there are four available configurations:

- Multiple-Input, Multiple-Output: MIMO.
- Single-Input, Multiple-Output: SIMO.
- Multiple-Input, Single-Output: MISO.

- Single-Input, Single-Output: SISO.

The utilization of multiple antennas in transmission and reception is known to greatly enhance the range and capacity of wireless communications in particular spatial directions. This is mainly done by exploring the multipath propagation phenomena, namely by reducing the impact of the deep fades, which consequently increases the robustness of the communication link. Another interesting feature of MIMO systems is that they allow for the simultaneous (parallel) transmission of multiple data streams, enhancing data throughput. Interference reduction is also a great feature in MIMO systems. This feature is supported by the fact that a multiple antenna receiver can by separate signals by using different spatial signatures, thus avoiding interference due to frequency reuse. Still regarding interference mitigation, one can consider a multiple antenna transmitter able to direct the transmitted signal to a given receiver, thus reducing the amount of distortion generated by other users. These techniques are usually collectively denoted as "beamforming" and usually present adaptive features [29].

However, these features cannot usually be explored simultaneously. In fact, there is a trade-off between diversity in transmission and multiplexing, as it is not possible to have optimal signal-to-noise ratio (SNR) and maximum spectral efficiency at the same time. Another problem of MIMO is the computational complexity of receiver decoding algorithms, which is related to their signal processing operations [30]. These topics are discussed in the next section.

2.2.1 Benefits

The diversity gain is associated with the mitigation of signal fading to obtain improved SNR. Signal-to-Noise Ratio is simply the ratio between the power of a received signal and noise power. Diversity is attained by employing multiple antennas in transmission and or reception. The same signal is sent by these antennas and is captured by the receiving element. Therefore, there a given signal is transmitted through several fading paths, which increases the probability that one of them does not experience a deep fade, hence enhancing the chance of a better overall SNR.

There are three types of diversity:

- Spatial Diversity.
- Frequency Diversity.
- Time Diversity.

Diversity gain in spatial diversity is attained when there is a low correlation between neighboring antenna element signals. Antenna elements should be sufficiently separated for this to happen, otherwise, it will translate into correlated signals between adjacent antenna units and they do not experience independent fading, reducing diversity gain.

This distance between elements is called coherence distance. We can call a channel "space selective" when the space between adjacent antennas is greater than the coherence

distance [31]. In a rich multipath environment, meaning that the signal might suffer alterations due to scattering obstacles in an environment that give rise to many propagation paths, is where we can extract the most benefit from "Spatial Diversity". It is known that for Base Stations in urban environments, the distance of half of a wavelength is enough to have a low correlation between neighboring antennas and achieve a "space selective" channel with high diversity gain [29].

Frequency diversity on the other hand relies on the transmission of the same signal by multiple antennas in different frequencies at the same time. Given that our objective is to combat signal fading, we should establish a bandwidth, commonly called coherence bandwidth, in which it is assumed that over its range, the channel frequency response is approximately flat [31].

Like in spatial diversity, when dealing with a rich multipath environment, each symbol is received multiple times due to the nature of electromagnetic waves and the way the signal can scatter, reflect and refract in these environments. Thus, these signals come with a delay between each other due to the reasons previously given. Hence the coherence bandwidth is given by the inverse channel delay spread [32].

Time diversity is achieved when the same signal is transmitted multiple times with a delay between each version. Like frequency and spatial diversity, here we have the same goal, namely enhancing the link SNR by introducing redundancy in the system. This delay is called "coherence time" and is usually calculated using the Channel Impulse Response (CIR), which can be calculated with the different amplitudes and phases of the channel taps. Coherence time is the duration in which the channel is assumed to be constant. This parameter depends on carrier frequency and mobility of UE which is always change. This can also be approximated to the inverse of the maximum Doppler frequency [31].

Multiplexing Gain can be achieved at the expense of diversity gain. To achieve some multiplexing gain we must have multiple antennas both in transmission as well as in reception. By using MIMO with spatial multiplexing, our goal becomes increasing data rates instead of signal reliability as when we employ diversity. If we consider a MIMOsystem with M transmit antennas and N receive antennas, it can be shown that the capacity of the system grows linearly with $min\{M, N\}$ [29].

At the transmitter, the data stream is split into M streams and simultaneously transmitted in a rich scattering environment using the same frequency band. The signal is then received and recombined to form the original message. In fact, by using multiple antennas to transmit sections of the original signal, we forfeit some of the redundancy we had due to diversity in the transmission, hence there is a trade-off between the two.

Interference can be accredited to many things, but in MIMO systems, it is usually an issue of frequency reuse causing it. This interference can degrade communication efficiency, which is justified by a low SNR and, consequently, a lower capacity. A way to effectively decrease inter-channel interference and signal correlation is to transmit the signal and direct it directly to the chosen users, using the so-called beamforming techniques. By directing the respective signal to each user, the amount of inter-user

interference in the system is decreased, and beamforming can effectively be seen as a spatial filter. In fact, beamforming is responsible for increasing capacity, by increasing SNR and decreasing interference, and multi-path fading, but also contributing to interference rejection.

Interference rejection is one of the main topics of this thesis project, given that this thesis is focused on the benefits that beamforming in the near-field can provide in terms of physical layer security. Another great inherent feature of beamforming is the ability to isolate the listener from evil eavesdroppers that might want to spy on crucial information. In fact, interference rejection or jamming rejection are very important topics when it comes to the security of wireless communications. Given the physical properties of the waves and the nature of the near-field, it has been shown that beamforming can have a focusing effect, which can be an interesting feature for increasing the physical layer security.

2.2.2 Challenges

As mentioned before, all benefits of MIMO come at a price. There are several challenges that can arise in MIMO communications. Problems such as dealing with the inherent trade-off between multiplexing gain and diversity gain, like those previously discussed, are still a hot research topic and still require further investigation.

As previously discussed, multiple antenna systems have been employed to combat channel frequency selective fading, by increasing the number of paths the signal takes from the BS to the UE in the downlink scenario. By transmitting several replicas of the same signal, we could, in theory, have a better chance of receiving the transmitted signal at the UE without a deep fade. This is what is called diversity gain. In a parallel line of thought, it was found that the channel fading, that "Transmit Diversity" and "Receive Diversity" were trying to eliminate, actually increases the Degrees of Freedom (DoF) for wireless communication purposes by [33], [34]. This means that, transmit-receive antenna pairs have independent fading channels, hence, they also have different path gains, allowing for the transmission of independent streams of information. This is what is known as multiplexing gain if the parallel streams are used to complement each other at the receiving end enhancing capacity. However, maximizing diversity gain does not necessarily maximize multiplexing gain. In [35], it was found that full diversity gain was achieved at the expense of capacity and multiplexing gain.

Other challenges like channel estimation come with dilemmas, such as pilot contamination and the use of computational costly and time-consuming calculations in the BS for precoding techniques [36]. The ones that have been more studied in the last years are:

- Channel Estimation: In a MIMO system, the channel between the transmitter and receiver consists of multiple complex channels, one for each pair of antenna elements. Estimating these channels accurately is crucial for achieving good performance, but it can be difficult due to noise, interference, and other factors.

- Interference management: MIMO systems often suffer from interference between the different antenna elements, which can degrade performance. Techniques such as precoding and beamforming can be used to manage this interference and improve performance.
- Synchronization: MIMO systems often require precise synchronization between the transmitter and receiver in order to achieve good performance. This can be challenging in dynamic environments or in systems with large numbers of antenna elements.
- Complexity: MIMO systems can be complex to design and implement, especially for systems with large numbers of antenna elements. This can make them more expensive and difficult to deploy.

The Channel State Information (CSI) is the channel response of mobile communication. It can be used by the receiver to optimize its signal processing algorithms, such as beamforming or equalization, in order to improve the performance of the communication system. In MIMO systems, CSI is required for communication, either for precoding or detection in the uplink and downlink respectively [37]. The way we attain this information is mostly by transmitting training sequences, namely through the so-called pilot signals.

In a MIMO communication system, a pilot signal is a known reference signal that is transmitted frequently from the transmitter to the receiver. The receiver uses the pilot signal to estimate the CSI between the transmitter and the receiver. The pilot signal is typically a low-rate, narrowband signal that is transmitted continuously or at regular intervals. It is designed to be robust against noise and interference and to be easy to detect and estimate at the receiver.

Let us talk about Duplexing methods. For MIMO communication systems, the relevant ones we shall talk about are Frequency Division Duplexing (FDD), and Time Division Duplexing (TDD), as this might influence the reciprocity of the estimated channel, as we will see [38].

In the FDD paradigm, the transmitter, and receiver use different frequencies for both the uplink and downlink channels. Analogous to cellular networks that use different frequency bands for different users to transmit and receive each stream of data from BS to UE and vice-versa, in FDD we can use the downlink and uplink channel simultaneously without interference as they do not share the same frequency band [39]. In a TDD system, the transmitter, and the receiver use the same frequency band for both the uplink and downlink channels. However, to avoid interference, they transmit at different time slots. The uplink and downlink channels are interleaved in time, using a defined time-division schedule [39].

If we use FDD, the uplink channel estimation is done at the BS with all users sending different spread code pilot sequences. For the downlink, it is more complex, a two-step process is necessary - As the BS transmits and assigns pilot symbols for the users, all the users answer back with an estimation of the CSI. Therefore, the time we reserve for

channel Estimation in the downlink increases with the number of antennas at the BS and this means that channel estimation might require a lot of processing power and time [37]. This can be somewhat avoided with TDD, as we can assume channel reciprocity, hence only uplink CSI needs to be estimated. However, this is not without downsides, as there are many for TDD, such as complexity due to the coordination and synchronization of the transmit and receive cycles of the uplink and downlink, and interference, since the uplink and downlink share the same frequency spectrum.

In TDD, it is assumed channel reciprocity to minimize pilot overhead, hence we only transmit pilot reference signals in the up-link. Usually, BS estimates channels based on Least Squares (LS) or Linear Minimum Mean Squared Error (LMMSE), a linear estimator that minimizes the Mean Squared Error (MSE) between the estimated CSI and the true CSI. It provides good performance in the presence of noise and has relatively good convergence properties paired with low computational complexity. With LMMSE, the CSI is estimated by joining the received signal with a set of known pilot signals that have been transmitted by the transmitter [37], [40].

As aforementioned, all of these techniques require the use of pilot sequences. However pilot signals are prone to contamination, this drawback is promptly known as pilot contamination. In fact, if pilot signals from different users are not perfectly orthogonal in frequency or time, they can interfere with each other, resulting in pilot contamination. This can lead to a wrong estimate of the CSI causing performance degradation of the overall system [40].

Hardware impairments are also an issue in MIMO systems and studies have shown that hardware impairments might cause lower performances and lead to erroneous channel estimates [36], [39]. Other relevant issues are:

- Power consumption: MIMO systems often require more complex signal processing and additional antennas, which can increase power consumption [39].
- Cost of Implementation: MIMO systems can be more expensive to implement due to the additional antennas and signal processing required.

In general, adding more antennas to a system will increase its cost. This is because each additional antenna requires additional hardware such as Radio Frequency (RF) components, cables, and amplifiers, as well as additional design and engineering efforts to integrate the antenna into the system. However, the cost increase may be offset by the improved performance and capabilities of the system. For example, a 6G system with a larger number of antennas may be able to provide higher data rates that justify the additional cost.

It is also important to consider that the energy consumption of a MIMO system will depend on the intended use and application of the system. For example, a MIMO system that is designed for use in high-bandwidth, low-latency applications may have a higher energy consumption than a system that is designed for use in low-bandwidth, low-power applications. Overall, the energy consumption of a MIMO system will depend on the

specific design and implementation of the system and the intended use and application of the system.

2.3 MIMO with Extremely Large Antenna Arrays

In the field of wireless communications, an antenna is a device that converts electromagnetic waves into electrical signals and vice versa. Antennas can be classified as active or passive, depending on whether they require an external source of power to operate.

An active antenna is an antenna that contains an amplifier, which boosts the signal received by the antenna. This type of antenna requires an external power source, such as a battery or a power outlet to operate. Active antennas are often used in situations where the signal strength is low, or when the antenna needs to transmit over long distances. A passive antenna, on the other hand, does not contain an amplifier and relies solely on the incoming electromagnetic waves to produce a signal. Passive antennas do not require an external power source to operate and are often used in situations where the signal strength is already high, or when the antenna only needs to transmit over short distances [41], [42].

In the context of 6G communication systems, active and passive antennas will play an important role in the design and operation of the network. 6G is expected to deliver faster data rates and lower latency than previous generations of wireless communication systems [12], and the choice of active or passive antennas will depend on the specific requirements of the system.

A reconfigurable intelligent surface is a type of antenna array that can dynamically change its properties in response to the surrounding environment. This allows the RIS to adapt to different channel conditions and improve the performance of the MIMO system [42]. A RIS is typically made up of a large number of passive elements, such as metal rods or patches, arranged in a grid or array. Each element can be individually controlled, allowing the overall shape and characteristics of the RIS to be modified. For example, the elements can be used to focus the radiation pattern of the antenna in a specific direction or to create a specific phase shift across the array by adjusting the impedance of the circuit [42]. In MIMO systems, a RIS can be used to improve the performance of the system by creating multiple communication paths between the transmitter and receiver, in the case where we do not have Line of Sight (LoS). This can be done by carefully controlling the phase of the received signal and by retransmitting it from the different elements of the RIS and, theoretically, makes it possible to increase the capacity of the MIMO system [42], [28]. However issues such as “multiplicative fading” turn this into a difficult task - As the path loss felt from the signal received from the RIS is the product of the path loss felt between UE to LIS and the path loss of the channel between LIS and BS, in an uplink paradigm. This makes it a lot bigger than otherwise it would be if we had an LoS type communication [42].

On the other hand, we could take a look at the paradigm of active elements in ELAA development, which are the so-called large intelligent surface. Contrary to the RIS, LIS are formed by active antenna elements that are able to transmit and receive information, this is exemplified in figure 2.3.

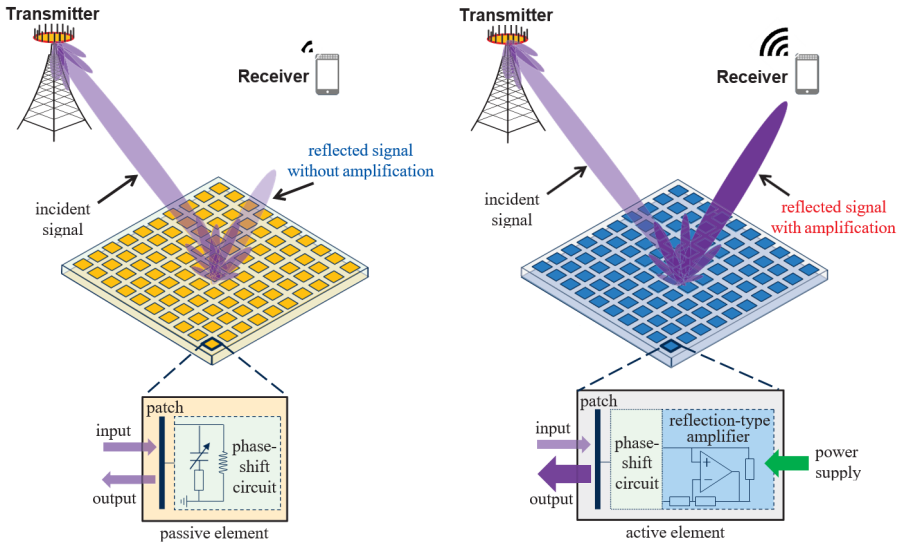

Figure 2.3: Reconfigurable Intelligent Surfaces (passive elements) versus Large Intelligent Surfaces (active elements) [42].

Similar to a RIS, large intelligent surfaces can emit and direct a signal by shifting its phase [42]. Like RIS, a LIS is also a type of antenna array that can dynamically change its properties in response to the surrounding environment to satisfy a given connection - Typically made up of a very large number of antennas, these elements are thought to occupy future building facades near high foot traffic areas, such as plazas, events, etc [28].

Given the naturally high available bandwidth provided by the untapped frequency bands and the current development of ELAA indicates that most of the communication done by these array configurations might occur in the near-field. More concretely, in the radiative near-field (also known as Fresnel region) as opposed to the traditional far-field operation. The far-field regime distance is lower bounded by the Fraunhofer limit [43]. Considering that D is the diagonal of the array at hand and λ is the wavelength, both these regions can be defined by:

$$d_{\text{Fresnel}} = 0.62\sqrt{\frac{D^3}{\lambda}} \qquad (2.1)$$

$$d_{\text{Fraunhofer}} = \frac{D^2}{\lambda} \qquad (2.2)$$

In radiation and propagation, it is known that electromagnetic waves propagate in a spherical fashion. However, due to the distance in far-field models, a given spherical wavefront can be approximated by a planar wavefront over a given receive antenna. Nevertheless, this approximation no longer holds in the radiative near-field region, where

the wave's curvature should be considered. This is further schematized in figures 2.3 and 2.3.

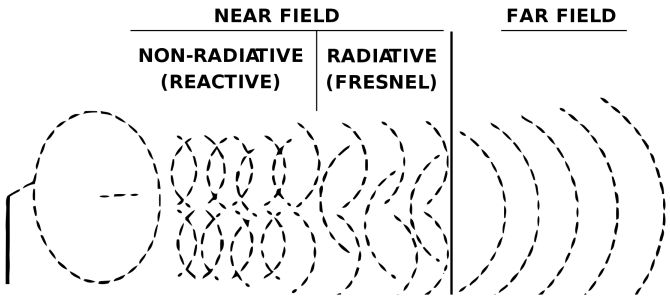

Figure 2.4: The relative Fresnel and Fraunhofer region

This physical property can be exploited for determining the users' location due to the different phase shift values of the antenna in the arrays from the spherical signal, allowing a decrease in the amount of signaling done for synchronization purposes [28].

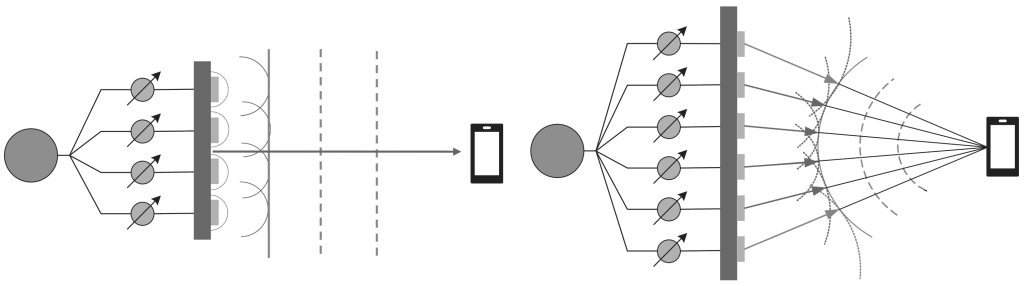

Figure 2.5: The planar wavefront approximation in the far-field versus The spherical wavefront in the near-field[28]

In the classical far-field channel models, the propagation distance between the different antennas of the array and the UE is approximately equal, leading to a similar path gain. In the near-field channel model, due to the distance between the array and the UE being shorter, this model no longer holds, since we will experience significant phase and angle of arrival differences. Therefore, due to this non-stationary channel paradigm, traditional fading models no longer hold.

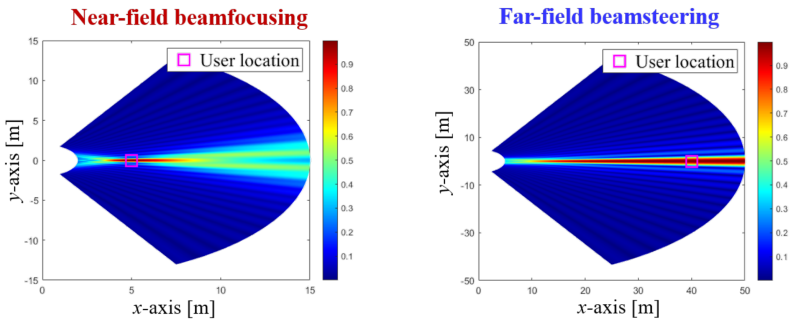

Figure 2.6: Normalized signal energy in near-field beamfocusing versus far-field beamforming [44].

It is thought that 6G communications can benefit, although with possible drawbacks, from near-field type propagation communication schemes.

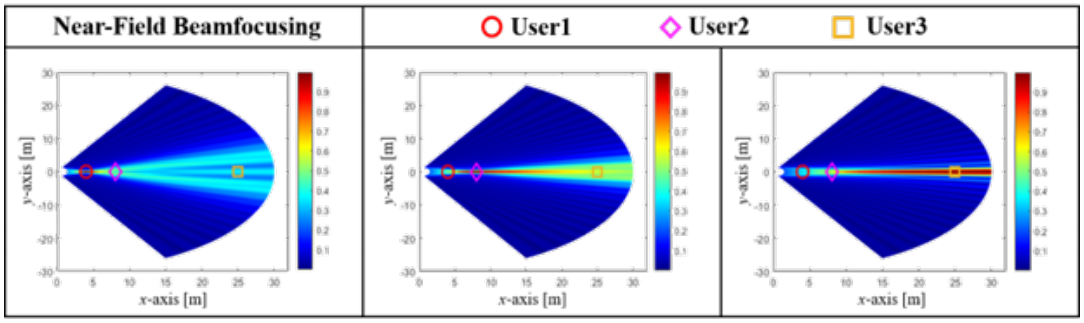

Figure 2.7: Multiple users served at the same angle - Spectral Efficiency with SDMA [44]

Possible capacity enhancements can happen with the transition from far-field to near-field. The increase in degrees of freedom in near-field makes it so we can have a spatial multiplexing gain by transmitting simultaneous parallel streams of data thanks to MIMO precoding. In [45], it was shown that the observed DoF in near-field are inversely proportional to the distance between UE and BS, and increase with BS and UE array aperture. This conclusion was also obtained in [46].

Another way we could benefit from near-field propagation is by using Space Division Multiple Access Space Division Multiple Access (SDMA) and increasing spectral efficiency. In SDMA, different user communication streams are able to share the same time and frequency [44]. For example, we could imagine a scenario depicted in figure 2.3 where in far-field users located in the same direction would experience immense interference with SDMA, has exemplified by figures 2.3 and 2.3. On the other hand, beamfocusing might be able to serve multiple users at the same angle at different distances from the BS. In [47], this possibility was tested and further developed and the results demonstrated that communication in the near-field can enhance multi-user accessibility.

2.4 Physical Layer Security

Wireless communication networks play a crucial part in daily activities. They are widely used by civilians and corporations alike, even military operations require the use of wireless applications, and with that comes the push to turn our communications as safe as possible from malicious users. Malefactors may attempt to disrupt communications by launching several attacks to access and destroy private information, or even try to shut off communication flow entirely.

Most contemporaneous security methods rely on so-called "Cryptographic Techniques", which are usually implemented on the higher layers of the Open System Interconnection model, for example, the Data Encryption Standard, where a common private key is shared by two users, colloquially called Alice and Bob, for A and B. However if these two users do not have access to this key, a secure private channel is needed to make this initial key

agreement. Here physical layer security techniques are central to the discussion, where a wireless communication channel between Alice and Bob must be established in order to supply the upper layer security and privacy algorithms of their fundamental common keys, hence turning Eve, the eavesdropper, and other malicious users jobs harder to decipher Alice and Bob's communication.

Some examples of passive attacks are disruptions such as eavesdropping and Traffic analysis, where the malicious user taps silently into to communication stream, active attacks are Denial of Service (DoS), message modification attacks, and many others. Secure wireless communications need to fulfill certain requirements [48], these are in place to guarantee the medium is protected from passive and active security threats:

- Authentication & Non-Repudiation: Authentication is the process of verifying that a device or user is who they claim to be. In wireless communication, authentication is important because it helps to ensure that only authorized devices or users are able to access the network. Non-repudiation, on the other hand, is a security measure that ensures that a device or user cannot deny having performed a specific action or transaction, like sending or receiving a message. This is often accomplished through the use of digital signatures that allow the sender to be uniquely identified and connected to the message they have sent. Novel technologies involving blockchain techniques are being tested in these environments [49], [50].
- Confidentiality and Access Control: Confidentiality refers to the protection of information from being accessed by unauthorized users or devices. This is mostly achieved through the use of encryption, which is the process of encoding data in such a way that it can only be accessed by someone with the appropriate decryption key. Even if the connection is being passively tapped into, it being encrypted protects its private content from the malicious eavesdropper. Access Control, on the other hand, is the process of filtering users that are able of accessing a private communication stream of information. This is mostly accomplished through the use of authentication techniques like access control lists, which determines which users or devices are allowed to access specific resources [49], [51], [52].
- Integrity and Availability: Integrity in communication, refers to the protection of the content of the original messages from unauthorized parties that might attempt to actively attack the data stream with message modification attempts to modify or tamper the original data. This is important because if the information is not protected from tampering, it may become unreliable or untrustworthy. Availability is about giving authorized devices or users to access the data and information they need at any specific time. This is basically ensuring the availability of the system to trustworthy third parties [49], [52].

The next two requirements are very important in the scope of this thesis, as they are a match for the novel near-field physical properties we are studying:

- Jamming Resistance: Resistance to jamming refers to the ability of a wireless communication system to continue active in the presence of interfering signals that attempts to disrupt the original signal. Jamming is a type of active attack in which the malicious user transmits a signal in the same frequency band and at the same time as the legitimate communication it is trying to disrupt. The main goal is to create noise and makes it difficult for the communication to be understood by the legitimate user. There are two types of jammers, active and reactive jammers. An active jammer will continue to broadcast its signal in hopes to disturb a target communication, on the other hand, a reactive jammer will only cast its signal when it detects the communication happening [49].
- Resistance to Eavesdropping: Resistance to eavesdropping refers to the ability of a communication system to safeguard the confidentiality of transmitted information by preventing unauthorized interception and access. Eavesdropping can be a significant threat to the security of wireless communications, as it can allow attackers to gain access to sensitive information [49], [53].

We can identify four major paradigms in terms of physical layer security schemes against different attacks:

- Power Approaches.
- Coding Approaches.
- Channel Approaches.

Communication protection can also be done with power-related approaches. An example is the use of a directional antenna. In [54], the performance of omnidirectional and directional antennas was compared under jamming conditions. It was observed, due to the presence of jamming, that omnidirectional antennas are not able to receive information as directional antennas can. This happens because the beamwidth is inversely proportional to the peak gain in a directional antenna. Another type of power-related approach is the introduction of artificial noise. The main idea of this technique noise is to transmit noise to the malicious user channel, therefore protecting the communication [49].

Other approaches, such as coding ones, are mainly used to enhance protection measures against jamming and eavesdropping. Error Correction Coding can be used to determine the number of redundant bits needed to protect the information based on the channel conditions, in order to achieve high efficiency. Here, efficiency is measured as minimizing mutual information between the receiver and the eavesdropper or maximizing it between the transmitter and receiver. Spread Spectrum Coding is a technique that involves the use of a wideband frequency spectrum to spread the signal information over a large frequency range, making it more difficult for an unauthorized receiver to intercept and decode the signal. Spread spectrum coding has two main types: Frequency Hopping Spread Spectrum (FHSS) and Direct Sequence Spread Spectrum (DSSS). FHSS transmits

the signal by rapidly changing its frequency among a predetermined set of channels. DSSS spreads the signal over a wide frequency range by adding a high-rate pseudo-noise code to the signal [55].

The following techniques exploit channel characteristics in order to increase security. RF fingerprinting relies on the extraction of Radio Frequency characteristics of the transmitter-receiver channel, each user generates a unique identifier derived from received and sent packets, this system monitors the evolution of each fingerprint, issuing an alert in case of a strange fingerprint being detected [49].

Algebraic Channel Decomposition Multiplexing Precoding is also a very interesting technique, as it denies the possibility of malicious users acquiring the true messages due to the difference in location between the legitimate user and the intruder, thanks to the Singular Value Decomposition (SVD) of the correlation matrix, which describes the channel between the transmitter and receiver.

The Randomization of MIMO Transmission Coefficient is also used as a form of physical layer security. In this technique, the transmitter generates a diagonal matrix dependent on the communication channel. This matrix is easily detectable for users that share the channel and undetectable for other users who don't, leading to a blind deconvolution problem due to the redundancy of channel reciprocity in MIMOsystems [55], [56].

3

Near-Field MIMO Communications

When an antenna radiates a signal, its electromagnetic profile can be mapped using Maxwell's equations. These equations are a strong mathematical tool and can be used for many applications such as classical optics and radio technologies [57].

In this section, it is provided a detailed analysis of the mathematical representation of the wireless communication channel. However, before we delve into this topic, it is crucial to first gain an understanding of the underlying principles that will enable us to navigate through this thesis. In the subsequent sections, the three main propagation regions will be analyzed, namely: The reactive near field, the radiative near field, and the far field. These field regions represent distinct areas where signals propagate in different ways, and it is crucial to characterize them for deriving accurate channel models.

We will begin by discussing the reactive near field, which is the region closest to the transmitter. Next, we will discuss the radiative near field, which is the region beyond the reactive near field. This is the region of interest in this study as it will be the primary focus of the potential for PLS applications. After that, we will delve deeper into the wave curvature effects on communication and examine current channel models performance that are based on the approximation of the Friis' formula and compare them to our wave curvature phase accounting model. As it will be demonstrated, the derived channel model should be precise enough to account for the phase differences in the impinging wavefront and this level of precision is not possible with the conventional far-field assumptions. However, we will also see that our model, when accounting for far-field type communications, will converge into the Friis approximation. This proves to be an excellent characteristic of the derived model and shows its accuracy for different field regions. Moreover, according to published research, antenna gain is significantly reduced when utilizing a far-field antenna propagation model for near-field communications, hence the need for a near-field model [58].

Finally, the far-field region is analyzed. This region is the farthest from the transmitter. By the end of this subsection, we hope to have provided a comprehensive overview of the main regions in wireless communication and their associated concepts. With this foundation, we can proceed to develop a mathematical model for wireless signal

propagation that incorporates all these factors. Also, this comprehensive overview will be accompanied by a thorough explanation of the impinging wave curvature. The concept of wave curvature is closely related to the propagation distance in wireless communication.

When electromagnetic waves are emitted from a transmitter, they propagate with spherical wavefronts and the distance from the source affects the accuracy of the approximations we make in our mathematical model. When the receiver is closer to the transmitter, the effects of wave curvature are more significant, and we must account for them. This is particularly important for near field communications [57], [59]. In these regions, the signal behavior is primarily influenced by the electromagnetic waves that propagate from the transmitter, and the wave curvature can significantly affect the signal's properties. However, for far-field communications, there is no need to consider wave curvature. This is because at greater distances from the transmitter, the wavefronts can be approximated as plane waves, and the effects of wave curvature become negligible, has in figure 3 shows. In the far-field region, the signal's behavior is primarily influenced by its power density, and other factors such as directivity are more important [58].

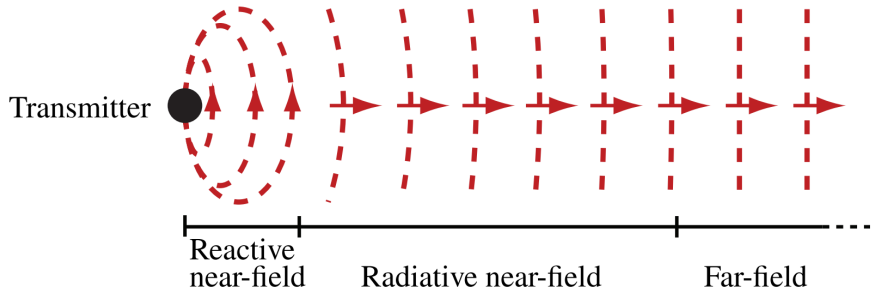

Figure 3.1: In the far field, the waves are approximately planar. However using an ELAA, users could be in the near field, and wave curvature cannot be neglected [59].

As previously stated, these three regions are defined by irregularities in the transmitted wavefront. The reactive near field is characterized not only by significant phase shifts but also by amplitude disparities between the transmitting wavefronts, given the short propagation distances. In the radiative near field, the region where we will dedicate the most attention, the amplitude disparities are no longer significant. However, the channel model should capture the phase shifts. Finally, in the far field, both the amplitude and phase variations are negligible and the uniform plane wave approximation is accurate [58], [59].

3.1 Phase Variations and Reciprocity

In the remainder of this thesis, it is considered that the communication is established between a large aperture antenna array and a user with a single isotropic antenna. Given we consider reciprocity, as briefly mentioned before, the downlink or uplink aspect of the

communication does not influence the next calculations and derivations, i.e., the channel is assumed to be equal for both communication directions.

From now on, we will simply refer to the reactive near field and the radiative near field as the near field for the sake of convention. As the frontier between the reactive near field and the radiative near field is not relevant for this case and our area of study focuses mainly on the radiative near field and the far field.

Let us start by considering the downlink of the communication from the point of view of the ELAA. Here, the transmit antenna has an aperture made up of a continuous stream of point sources that are all capable of emitting components of spherical waves. This can be the case because the antennas are electrically small and closely spaced, hence, integrals over the aperture can be used to study propagation effects rather than summations of individual antennas.

When viewed from a sufficiently long distance, the combined wavefront can appear to be planar. The electric fields produced by several point sources are superimposed in this area, which is referred to as the far field. The strength of the far field is inversely proportional to the propagation distance because the angle is the only factor that may alter the proportionality constant [58], [59].

Now, let us consider the other way around, i.e., the uplink direction. To find out for which distances the phenomenon occurs, we will consider the single isotropic antenna as the transmitter and the ELAA as the receiver. The ELAA is composed of $N = 1$ aperture antenna elements and is represented as having a maximum length D, such as depicted in figure 3.2. Due to the sufficient distance, the electric field's amplitude over the receive antenna should be constant in the far field, with the distance having no bearing on the phase fluctuations, which solely rely on the incidence angle [59].

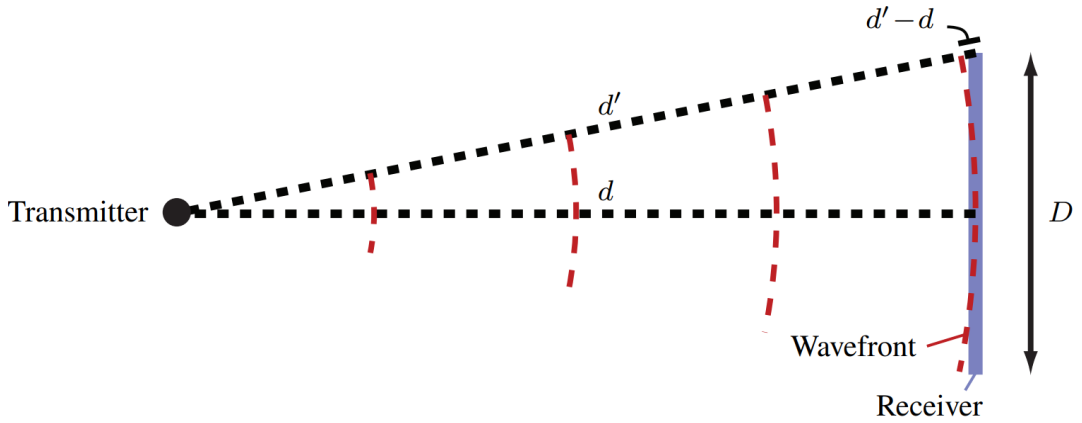

Figure 3.2: There is a delay between the center of the receiver and the edge due to the curvature of an impinging spherical wave. This delay becomes a phase-shift [59].

In literature, it is agreed that the maximum phase shift between the center of the array and its edges can be should be below $\pi/8$ so that the far field assumption is valid, this

means that the phase would not vary by more than $\pi/8$ radians over the array's aperture [60]. Note that the phase shift is

$$\frac{2\pi}{\lambda}(d' - d) = \frac{2\pi}{\lambda}\left(\sqrt{d^2 + \frac{D^2}{4}} - d\right) \approx \frac{\pi}{4}\frac{D^2}{\lambda d}, \tag{3.1}$$

where d is the distance between the transmitter and the center of the array, d' is the distance between the transmitter and the edge of the array and D is the size of the receiver array. By denoting d_F as the propagation distance and equating it to the maximum allowed phase shift of $\pi/8$, we obtain what is called the Fraunhofer distance (also known as Rayleigh distance) [61]. This distance is given by

$$\frac{\pi}{8} = \frac{\pi}{4}\frac{D^2}{\lambda d_F} \rightarrow d_F = \frac{2D^2}{\lambda}. \tag{3.2}$$

We consider an ELAA composed of many small antennas (i.e., each antenna is relatively small when compared with the wavelength). Collectively, all antennas form a large antenna aperture. The antennas have diagonal D. Since this array is composed of N antenna (where $\sqrt{N} \in \mathbb{N}$), the maximum dimension of the array is $D_{ELAA} = D\sqrt{N}$.

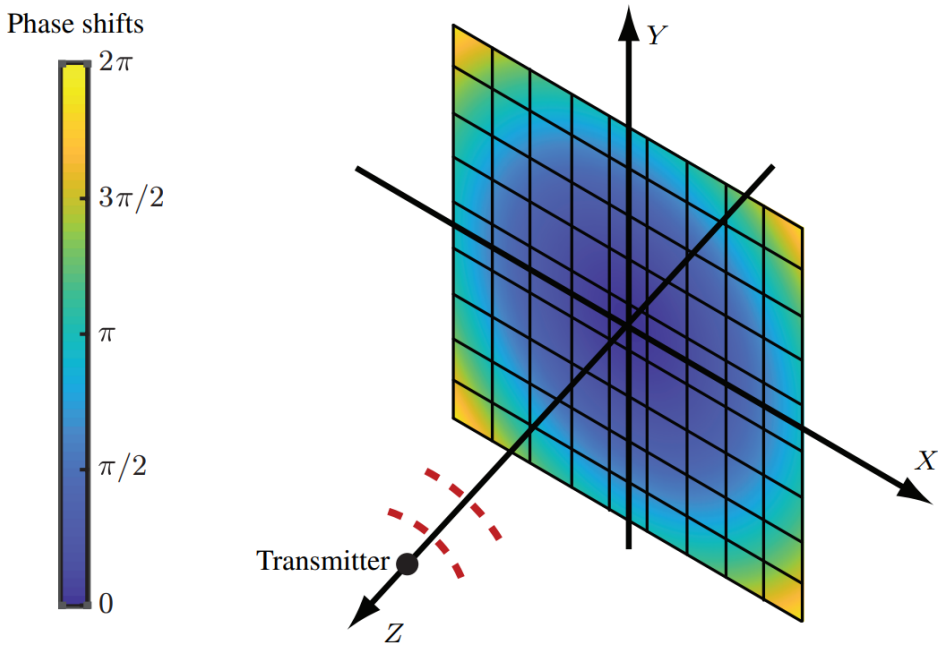

Figure 3.3: The circular phase changes over the ELAA caused by the spherical wavefronts are not negligible over the array. By using sub-wavelength-sized antennas this variation is negligible over each antenna, as it is lower than $\pi/8$ [59].

The circular phase variations over the ELAA are generated by the spherical wavefronts in the radiative near field and are depicted in figure 3.3. To overcome this adversity, sub-wavelength-sized antennas are employed to minimize the variation within each antenna.

By considering the $\pi/8$ phase-shift restriction for the whole array instead of the single antenna we get the Fraunhofer array distance, given by

$$d_{FA} = \frac{2D_{ELAA}^2}{\lambda} = \frac{2(D\sqrt{N})^2}{\lambda} = Nd_F. \tag{3.3}$$

From equation equation (3.3), it can be noted that the d_{FA} can be very large, or at least large enough to encompass a large area like for example, an indoor plaza of an airport where we expect a lot of traffic. As an example of this scenario, let us consider an array of $N = 11025$ antennas (i.e., $\sqrt{N} = 105$) where each antenna has a diagonal $D = 0.025m$. This leads to an array with total dimension A_{ELAA}= $3.44m^2$. Let's also consider that the carrier frequency is $f_c = 3GHz$. With these dimensions the Fraunhofer and Fraunhofer array distance are respectively $d_F = \frac{2D^2}{\lambda} = 0.0125m$ and $d_{FA} = \frac{2D_{\text{ELAA}}^2}{\lambda} = N\frac{2D^2}{\lambda} = Nd_F = 137.8125m$. It is also expected that the propagation distance is somewhere situated between the d_F and d_{FA}. In that scenario, the impinging wavefronts are approximately planes at the "antenna level" but the curvature cannot be neglected within the array.

In this study, we will consider both communication directions: The uplink and the downlink. To simplify the model, we will consider the channel between the user and ELAA as reciprocal. This is done by design and it is justified by the assumption of a TDD operation. Assuming reciprocity will allow the regions that are defined from the transmitter's viewpoint to also be perceived similarly from the receiver's perspective. To put it simply, if the wireless channel is reciprocal, the channel estimation can be done at one end of the communication link and used at the other end, since the same channel characteristics apply in both directions. Hence, for modeling reasons, the terms transmitter and receiver will and can be used interchangeably. Taking into account channel reciprocity can be highly beneficial as we tackle the significant challenge of identifying a channel model that takes wave curvature in the near field into consideration. By accounting for reciprocity, the channel estimation will remain consistent both in the uplink, where we will investigate the anti-jamming properties of ELAAs, and in the downlink, where we will examine eavesdropping.

Despite being less intricate and sub-optimal, the TDD communication paradigm between the ELAA and the user is preferred as it inherently possesses this property. This enables our model to be less demanding in terms of simulation requirements while still maintaining credibility and attaining consistent results. FDD is a communication method that involves dividing the available bandwidth of a communication channel into distinct non-overlapping frequency bands, with each band dedicated to transmitting a separate signal. These different frequency bands would, although slight, would cause inconsistencies in our model, as it has a direct dependency on propagation frequency, as we will see ahead. TDD, on the other hand, relies on timing and coordination between the user and BS. This drawback in this study is not taken into account, as we will focus on the uplink and downlink separately but always consider the same frequency band to maintain some level of consistency in the study. TDD is a communication mode that uses the

same frequency band for both uplink and downlink communication but at different time intervals. Hence, TDD is ideal for channel estimation reciprocity because it enables the transmitter and receiver to use the same frequency band at different times. Usually, with TDD, the receiver can estimate the channel characteristics during the uplink time interval and transmit the information to the transmitter during the downlink time interval. This information can be used by the transmitter to adjust its transmission parameters based on the current channel conditions, improving the overall performance of the wireless communication system [39].

The upcoming sections of this thesis present the derivation of a near-field channel model. Beginning with the fundamental Maxwell equations and assumptions, we will establish a tensor Green's function and then streamline the expression to meet our modeling requirements. Subsequently, we will extrapolate this model to the intended scenario, which will be extensively detailed in the following sections. This process will provide a comprehensive understanding of the near-field channel characteristics so that the wireless links can be simulated with accuracy and the beamforming algorithms designed correctly.

3.2 System Characterization

In this study, two scenarios are considered, namely: a Single Input Multiple Output (SIMO) system in the uplink and a Multiple Input Single Output (MISO) in the downlink. The UE is equipped with a single antenna terminal and communicates with the ELAA using a carrier with frequency f_c. It is assumed that the propagation speed of waves in free space is equivalent to the speed of light in a vacuum.

For the simulations, it is considered a 3D space where the ELAA is deployed in the YZ plane, as can be observed in figure 3.4. It is considered that the ELAA is centered on the origin of a rectangular coordinate system, and without loss of generality, it is also assumed that there is an odd number of antennas on each array side. As a consequence, the array has a central antenna. This array is composed of N edge-to-edge square aperture antennas and every antenna has a physical area A. Unless otherwise stated, it is assumed that the user is positioned along XY plane in $\underline{p_s} = (x_s, y_s, 0)$. Note that by considering that each square antenna of the ELAA has a side L, the area of each of these antennas can be calculated as $A = L^2$. Moreover, their diagonal is given by $D = L\sqrt{2}$. Therefore, the dimensions (side, diagonal, and area) of the ELAA are respectively given by:

$$L_{\text{ELAA}} = \sqrt{N}L, \tag{3.4}$$

$$D_{\text{ELAA}} = \sqrt{N}D, \tag{3.5}$$

$$A_{\text{ELAA}} = NA = N\frac{D^2}{2}. \tag{3.6}$$

By numbering the individual antenna from left to right, row by row from the top to the bottom, the center of the nth antenna is defined as $\underline{p_n} = (0, y_n, z_n)$. Note that since the

antennas that form the array are located in the YZ plane, x_n is always null. The receive points that form the region spanned by the nth antenna is defined as $\mathcal{A}_n = \{(0, y_n, z_n) : -\frac{L}{2} \leq y_n \leq \frac{L}{2}, -\frac{L}{2} \leq z_n \leq \frac{L}{2}\}$.

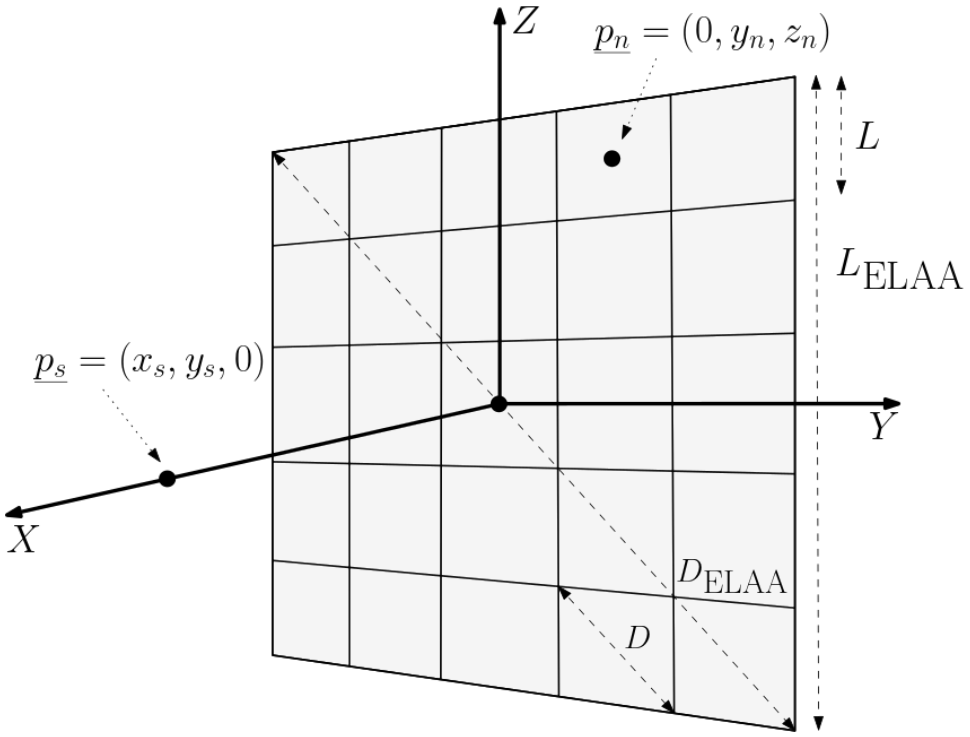

Figure 3.4: Considered scenario where an ELAA is deployed on the YZ plane.

The individual positions of the antenna can be computed by taking into account the individual dimensions of each antenna. More concretely, the coordinates of the center of the nth antenna are

$$y_n = -\frac{(\sqrt{N}-1)L}{2} + \mod(n-1, \sqrt{N})L, \tag{3.7}$$

where $\text{mod}(a, b)$ yields the remainder of an integer division of b by a and

$$z_n = \frac{(\sqrt{N}-1)L}{2} - L\left\lfloor \frac{n-1}{\sqrt{N}} \right\rfloor, \tag{3.8}$$

where $\lfloor \text{a} \rfloor$ is the floor function, which takes the input a and outputs the integer lesser or equal to it. The index corresponding to the central antenna is also given by the following equation

$$n_{center} = \frac{\sqrt{N}-1}{2}\sqrt{N} + \frac{\sqrt{N}-1}{2} + 1. \tag{3.9}$$

An ELAA has the potential to be installed at various locations where clear LoS communication with users can be ensured. The optimal placement of these prototypes could be on the ceiling of an office, eliminating the need for Ethernet cables and cable management,

while providing secure and high-speed communication to all occupants of the room. Additionally, ELAAs could be installed in the interior facade of an airport to accommodate high levels of traffic or even near public plazas for the same reasons.

As previously mentioned, the user positioned at $\underline{p_s}$ has a single isotropic antenna, which is different from the aperture antenna elements that compose the ELAA. An isotropic antenna is a theoretical antenna with no losses that radiates or receives electromagnetic waves equally in all directions. In other words, it has a radiation pattern that is perfectly spherical, with equal radiation intensity in all directions. It is a hypothetical antenna used as a reference to evaluate directivity of other antennas [62].

The radiation pattern of an antenna is a graphical representation of the directional properties of its electromagnetic radiation. In the case of an isotropic antenna, its radiation pattern is a perfect sphere. Figure 3.5 shows the radiation pattern of an isotropic antenna, considering horizontal and vertical perspectives.

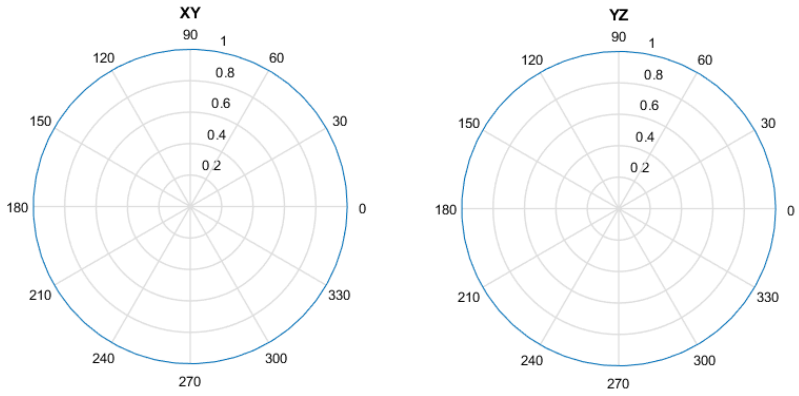

Figure 3.5: Two-dimensional representation of the radiation pattern of the isotropic antenna.

The choice of an isotropic antenna with unitary gain ($G = 1$) for the transmit antenna is related to the fact that the main goal is to evaluate the ELAA behavior. In fact, since we are studying the interaction between an isotropic radiator and an array of aperture antennas, the potential loss from directivity will be associated with the antenna array. The effective area of an antenna is defined as the ratio between the power available at the terminals of a receiving antenna and the power flux density of a plane wave that strikes the antenna from a particular direction, with the same polarization as the antenna. If no direction is specified, it is assumed that the direction with the maximum radiation intensity is being considered [62].

As mentioned before, the distance between the single antenna user and the ELAA is important to define the field region and, consequently, an adequate channel model that is able to capture the incident wave curvature that is experienced in the near field but also that captures the far field communication aspects that are expected for all channel response models, like the approximation of the Friis' formula. Not only will the distance between

the single antenna user and the ELAA change but also the number of total antennas in the system. As previously discussed, this directly impacts the Fraunhofer array distance in equation (3.3).

3.3 Channel Modeling

Accurately modeling the propagation characteristics of a communication link is crucial, especially when employing large antenna arrays. When communicating with an ELAA, the far field assumption typically utilized in modeling channel responses may not be valid. This is explained by the fact that although it is likely that the user is beyond the Fraunhofer distance of each antenna element, it might be below the Fraunhofer array distance. Within this range, the wave curvature along the individual antennas that make up the ELAA is minimal, at less than $\pi/8$, which is the definition of the near field. However, the impinging wave curvature along the entire array remains noticeable.

Having provided a comprehensive context for system characterization, let us now focus on the channel modeling issues. The next step involves the definition of the electric field at a particular location, which will later hinge on the relative difference between the locations of the transmit and receive antennas. This model is crucial to understand the channel characteristics and will form the basis for further analysis. Let's define $\mathbf{d}$ as the vector between two points in space such that

$$\mathbf{d} = \mathbf{r} - \mathbf{s} = (x_r - x_s)\hat{\mathbf{e}}_x + (y_r - y_s)\hat{\mathbf{e}}_y + (z_r - z_s)\hat{\mathbf{e}}_z = \Delta x\hat{\mathbf{e}}_x + \Delta y\hat{\mathbf{e}}_y + \Delta z\hat{\mathbf{e}}_z. \tag{3.10}$$

The two points in space, namely the source, and receiver, can be denoted as $\underline{p_s} = (x_s, y_s, z_s)$ and $\underline{p_r} = (x_r, y_r, z_r)$, respectively. The distance between these two points in space is

$$d = d(\underline{p_r}, \underline{p_s}) = ||\mathbf{d}(\underline{p_r}, \underline{p_s})||. \tag{3.11}$$

In the remainder of this thesis, it is assumed that the receiver is beyond the reactive near field of the transmitter. In the radiative regime, the curvature of the impinging wave should be considered and the channel responses should account for the individual effective area, pathloss, and polarization loss of each antenna element [63]. This requires the definition of the amplitude and phase of the electric field over the entire array, which contrasts with the conventional plane wave regime, where neither the variations of effective area nor the polarization losses are considered, and the channels are usually modeled with the simplified Friis' formulas [64].

The channel model will be compared with the model typically approximated using Friis' approximations. It is worth noting that as the distance between the communication nodes grows, the equations for both models will tend to converge to the same value. This is because Friis' formulas are only accurate for far field regimes and become less precise as the distance decreases. Therefore, by comparing the two models, we can better understand the limitations of Friis' approximations and the importance of using appropriate models

for different communication scenarios. Since the user has an isotropic transmit antenna, it can be shown that the electric field at a given location in space can be computed using Green's function

$$\mathbf{F}(\mathbf{d}) = -\frac{\mathrm{j}\omega\mu}{4\pi d}\left[\mathbf{I} + \frac{1}{k}\nabla\nabla\right]e^{-\mathrm{j}kd}, \tag{3.12}$$

where j is the imaginary unit and ω represents the angular frequency. Moreover, $\boldsymbol{I}$ represents an identity matrix, ∇ is the nabla operator and k denotes the wave number, which describes the number of complete wave cycles of an electromagnetic field that exist in one meter of propagation. Note also that $k = \frac{\omega}{c} = \frac{2\pi}{\lambda}$. Here c denotes the light speed in a vacuum, on the other hand, μ represents the permeability of free space and measures the amount of resistance encountered when forming a magnetic field in a classical vacuum. It is considered that the spherical wave travels between the locations $\underline{p_s}$ and $\underline{p_r}$ and the path length is given by equation (3.11).

By expanding equation (3.12), we can see that several terms in this formula are proportional to $\frac{1}{d}$ or to $\frac{1}{d^2}$. By developing this expression further, it results in

$$\mathbf{F}(\mathbf{d}) = -\frac{\mathrm{j}Z_0 e^{-\mathrm{j}kd}}{2\lambda d}\left[\left(\mathbf{I} - \hat{\mathbf{d}}\cdot\hat{\mathbf{d}}^H\right) + \frac{\mathrm{j}\lambda}{2\pi d}\left(\mathbf{I} - 3\hat{\mathbf{d}}\cdot\hat{\mathbf{d}}^H\right) - \frac{\lambda^2}{(2\pi d)^2}\left(\mathbf{I} - 3\hat{\mathbf{d}}\cdot\hat{\mathbf{d}}^H\right)\right], \tag{3.13}$$

where Z_0 is the free space impedance given by $Z_0 = \sqrt{\frac{\mu}{\epsilon}}$, with ϵ denoting the permittivity of free space. The normalization is done by dividing the vector by its norm $||\mathbf{d}|| = \sqrt{\Delta x^2 + \Delta y^2 + \Delta z^2}$, i.e., $\hat{\mathbf{d}} = \frac{\mathbf{d}}{||\mathbf{d}||}$. The resulting normalized vector, $\hat{\mathbf{d}}$, has unitary magnitude and points in the same direction as the original vector $\mathbf{d}$. Note also that $(\cdot)^H$ denotes the Hermitian operator which is equivalent to the transpose conjugate of a matrix or vector.

If the magnitude of vector $\mathbf{d}$ is equal to or greater than the wavelength, the receiving point can be assumed to lie beyond the reactive near field. In this scenario, if the distance between the point source of the electric field and the user is much greater than the wavelength of the propagated field ($||\mathbf{d}|| \geq \lambda$), the second and third terms of equation (3.12) can be neglected, resulting in the following approximation

$$\mathbf{F}(\mathbf{d}) \approx -\frac{\mathrm{j}Z_0 e^{-\mathrm{j}kd}}{2\lambda d}\left(\mathbf{I} - \hat{\mathbf{d}}\cdot\hat{\mathbf{d}}^H\right). \tag{3.14}$$

It should be noted that the dot product of the normalized direction vector by its Hermitian leads to the 3×3 matrix

$$\hat{\mathbf{d}}\cdot\hat{\mathbf{d}}^H = \begin{bmatrix} \hat{\Delta x}^2 & \hat{\Delta x}\hat{\Delta y} & \hat{\Delta x}\hat{\Delta z} \\ \hat{\Delta y}\hat{\Delta x} & \hat{\Delta y}^2 & \hat{\Delta y}\hat{\Delta z} \\ \hat{\Delta z}\hat{\Delta x} & \hat{\Delta z}\hat{\Delta y} & \hat{\Delta z}^2 \end{bmatrix}, \tag{3.15}$$

where $\hat{\mathbf{d}} \in \mathbb{R}^{3\times 1}$ and $\hat{\mathbf{d}}^H \in \mathbb{R}^{1\times 3}$. To obtain the individual components in each direction of the vector $\mathbf{d}$ of the Green function, the next step in the process involves subtracting an identity 3×3 matrix from the previous dot product, which leads to

$$\mathbf{F}(\mathbf{d}) \approx -\frac{jZ_0 e^{-\mathrm{j}kd}}{2\lambda d}\begin{bmatrix} F_x(\mathbf{d}) & F_y(\mathbf{d}) & F_z(\mathbf{d}) \end{bmatrix}. \tag{3.16}$$

The individual components of the $\mathbb{C}^{3\times3}$ matrix can be arranged in the format of the column vectors given by

$$\mathbf{F}(\mathbf{d}) \approx -\frac{jZ_0 e^{-\mathrm{j}kd}}{2\lambda d}\begin{bmatrix} 1-\hat{\Delta x}^2 & -\hat{\Delta x}\hat{\Delta y} & -\hat{\Delta x}\hat{\Delta z} \\ -\hat{\Delta y}\hat{\Delta x} & 1-\hat{\Delta y}^2 & -\hat{\Delta y}\hat{\Delta z} \\ -\hat{\Delta z}\hat{\Delta x} & -\hat{\Delta z}\hat{\Delta y} & 1-\hat{\Delta z}^2 \end{bmatrix}. \tag{3.17}$$

Since the only direction excited at the source is the positive Z axis, hence only the components weight by $\hat{\mathbf{e}}_z$ will be accounted for, which means that only $\mathbf{F}_z(\mathbf{d})$ contributes for the electric field. Therefore, only the following component of the Green function is of interest for the electric field computation

$$\mathbf{F}_z(\mathbf{d}) = -\frac{\mathrm{j}Z_0 e^{-\mathrm{j}kd}}{2\lambda d}\left[-\hat{\Delta x}\hat{\Delta z}\hat{\mathbf{e}}_x - \hat{\Delta y}\hat{\Delta z}\hat{\mathbf{e}}_y + (1-\hat{\Delta z}^2)\hat{\mathbf{e}}_z\right]. \tag{3.18}$$

The current density direction is determined by the physical layout of the antenna and the direction of the current flow in the antenna structure. The polarization of an antenna is the orientation of the electric field in the electromagnetic wave radiated by the antenna. In general, the polarization of an antenna is parallel to the direction of the current flow and the current density vector in the antenna structure. For example, a dipole antenna with a horizontal orientation will have a horizontal polarization, while a dipole antenna with a vertical orientation will have a vertical polarization. It is important to note that the polarization of an antenna is also affected by the orientation of the antenna relative to the receiving antenna or the polarization of the incident wave. If the receiving antenna is oriented in a different direction than the polarization of the incident wave, there may be a polarization mismatch, which can result in reduced signal strength. Hence the current density vector is described as $\mathbf{J}(\mathbf{s}) = J_x(\mathbf{s})\hat{\mathbf{e}}_x + J_y(\mathbf{s})\hat{\mathbf{e}}_y + J_z(\mathbf{s})\hat{\mathbf{e}}_z$, is given only by

$$\mathbf{J}(\mathbf{s}) = J_z(\mathbf{s})\hat{\mathbf{e}}_z. \tag{3.19}$$

Here, $\mathbf{s}$ and $\mathbf{r}$ are the affix vectors of $\underline{p_s}$ and $\underline{p_r}$, respectively. Under these conditions, only the third column of the Green's function $\mathbf{F}(\mathbf{d})$, which is defined as the $\mathbb{C}^{3\times3}$ column vector $\mathbf{F}_z(\mathbf{d}) = -\hat{\Delta x}\hat{\Delta z}\hat{\mathbf{e}}_x - \hat{\Delta y}\hat{\Delta z}\hat{\mathbf{e}}_y + (1-\hat{\Delta z}^2)\hat{\mathbf{e}}_z$, is used for the computation of the electric field.

$$\mathbf{E}(\mathbf{d}) = \mathbf{F}(\mathbf{d})\mathbf{J}(\mathbf{s}) = \mathbf{F}_z(\mathbf{d})\mathbf{J}_z(\mathbf{s}) = \mathbf{F}_z(\mathbf{r}-\mathbf{s})\mathbf{J}_z(\mathbf{s}). \tag{3.20}$$

Note that the channel only depends on $\mathbf{F}_z(\mathbf{d})$, while $\mathbf{J}_z(\mathbf{s})$ concentrates the impact of the transmitted signal. Moreover, since only the electric field perpendicular to the receive

antenna contributes to the channel, for an aperture deployed in the YZ plane, where the normal direction is $\hat{\mathbf{e}}_x$, the coupling coefficient between the source at and the receiving point is given by the following expression, i.e., the aperture antenna can only extract power from the component of the electric field impinging from $\hat{\mathbf{e}}_x$ (the normal direction). Hence, the electric field is reduced to a single component and is provided by the following simplification

$$c(\mathbf{d}) = \sqrt{4\frac{A_T}{Z_0^2}|\mathbf{F}_z(\mathbf{d})|^2\left(\hat{\mathbf{d}}\cdot\hat{\mathbf{e}}_x\right)}e^{-\mathrm{j}kd}. \tag{3.21}$$

By applying fundamental algebraic techniques, it is possible to manipulate the equation (3.21) in order to simplify the expression for the coupling coefficient that describes the connection between the source of the electric field and the receiver. Additionally, Green's function can be expanded and written in a manner that highlights the contribution of each directional component toward the coupling coefficient

$$\begin{aligned}
c(\mathbf{d}) &= \sqrt{4\frac{A_T}{Z_0^2}|\mathbf{F}_z(\mathbf{d})|^2\left(\hat{\mathbf{d}}\cdot\hat{\mathbf{e}}_x\right)}e^{-\mathrm{j}kd} \\
&= \sqrt{4\frac{A_T}{Z_0^2}\left(\left(-\hat{\Delta x}\hat{\Delta z}\right)^2+\left(-\hat{\Delta y}\hat{\Delta z}\right)^2+\left(1-\hat{\Delta z}^2\right)^2\right)\hat{\Delta x}}e^{-\mathrm{j}kd} \\
&= \sqrt{\frac{A_T}{\lambda^2 d^2}\left(\hat{\Delta x}^2+\hat{\Delta y}^2\right)\hat{\Delta x}}e^{-\mathrm{j}kd} \\
&= \sqrt{\frac{A_T}{\lambda^2}\frac{(\Delta x^2+\Delta y^2)\,\Delta x}{d^5}}e^{-\mathrm{j}kd} \\
&= \sqrt{\frac{1}{4\pi}\frac{(\Delta x^2+\Delta y^2)\,\Delta x}{d^5}}e^{-\mathrm{j}kd} \\
&= \frac{1}{\sqrt{4\pi}}\frac{\sqrt{(\Delta x^2+\Delta y^2)\,\Delta x}}{d^{5/2}}e^{-\mathrm{j}kd}.
\end{aligned} \tag{3.22}$$

We culminate in an expression that represents the coupling coefficient between the two entities in space. Further developments in the equation lead to the expanded form

$$c(\mathbf{d}) = c(\mathbf{r}-\mathbf{s}) = c(\Delta x,\Delta y,\Delta z) = \frac{1}{\sqrt{4\pi}}\frac{\sqrt{(\Delta x^2+\Delta y^2)\,\Delta x}}{(\Delta x^2+\Delta y^2+\Delta z^2)^{5/4}}e^{-\mathrm{j}k\sqrt{\Delta x^2+\Delta y^2+\Delta z^2}}. \tag{3.23}$$

3.3.1 SISO

The coupling coefficient refers to the impinging electric field. For this Single Input Single Output (SISO) scenario, the lossless isotropic antenna is located at $\underline{p_s}$ in the XY plane and transmits a signal that has polarization in the Z axis, as shown in figure 3.6. Moreover, an aperture antenna is placed at the origin, lying on the same plane as the YZ plane. The receivers surface is given by $\mathcal{A} = \{(0, y_r, z_r) : -\frac{L}{2} \leq y_r \leq \frac{L}{2}, -\frac{L}{2} \leq z_r \leq \frac{L}{2}\}$.

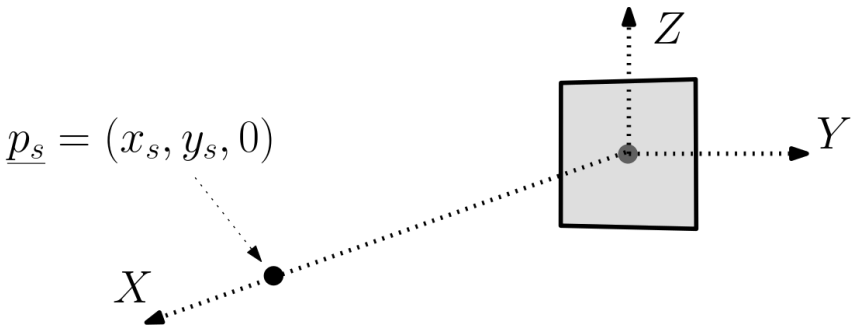

Figure 3.6: Depicted SISO scenario.

The general channel response over the receiver antenna is given by

$$h(\Delta x, \Delta y, \Delta z) = \sqrt{\frac{1}{A}} \int_{-L/2}^{L/2} \int_{-L/2}^{L/2} c(\Delta x, \Delta y, \Delta z) \partial \Delta y \partial \Delta z. \tag{3.24}$$

On the other hand, the channel gain is given by

$$|h(\Delta x, \Delta y, \Delta z)|^2 = \left| \sqrt{\frac{1}{A}} \int_{-L/2}^{L/2} \int_{-L/2}^{L/2} c(\Delta x, \Delta y, \Delta z) \partial \Delta y \partial \Delta z \right|^2. \tag{3.25}$$

The channel gain is dependent on Δx, Δy, and Δz. This dependence arises due to the integration process over the antenna aperture, which is positioned in the YZ plane. As a result of this integration, the vector $\mathbf{r}$ varies across the aperture, causing a change in the vector $\mathbf{d}$ specifically due to the variations in Δy and Δz. Additionally, the gain is influenced by the parameter Δx to account for the possibility of the user being located at $\underline{p_s}$ and having the freedom to move within the XY plane. This movement affects the vector $\mathbf{s}$, consequently impacting $\mathbf{d}$ as it relies on both Δx and Δy.

Let us now focus on the power gain. Here a unitary transmit antenna gain ($G_T = 1$) is implicit, since we are considering an isotropic antenna. In general, the receive antenna gain can be defined as

$$G_R(\Delta x, \Delta y, \Delta z) = \frac{\frac{1}{Z_0}\left|\int_{-L/2}^{L/2}\int_{-L/2}^{L/2} c(\Delta x, \Delta y, \Delta z)\partial\Delta y\partial\Delta z\right|^2}{\frac{\lambda^2}{4\pi}\frac{1}{Z_0}\int_{-L/2}^{L/2}\int_{-L/2}^{L/2}|c(\Delta x, \Delta y, \Delta z)|^2\partial\Delta y\partial\Delta z}$$
$$= \frac{4\pi}{\lambda^2}\frac{\left|\int_{-L/2}^{L/2}\int_{-L/2}^{L/2} c(\Delta x, \Delta y, \Delta z)\partial\Delta y\partial\Delta z\right|^2}{\int_{-L/2}^{L/2}\int_{-L/2}^{L/2}|c(\Delta x, \Delta y, \Delta z)|^2\partial\Delta y\partial\Delta z}. \tag{3.26}$$

The highest antenna gain is attained in the far field region. The perpendicular plane wave leads to [65]

$$G_M = \frac{4\pi}{\lambda^2}A. \tag{3.27}$$

The index "M", stands as maximum as it represents the maximum attainable gain in the far field. The maximum gain in a particular direction of incidence can only be achieved if the receiver is beyond the Fraunhofer distance. In order to normalize the gain, we shall define the normalized antenna gain as the ratio between equation (3.26) and equation (3.27)

$$\bar{G}(\Delta x, \Delta y, \Delta z) = \frac{G_R(\Delta x, \Delta y, \Delta z)}{G_M} = \frac{\left|\int_{\mathcal{A}} c(\Delta x, \Delta y, \Delta z)\partial\Delta y\partial\Delta z\right|^2}{A\int_{\mathcal{A}}|c(\Delta x, \Delta y, \Delta z)|^2\partial\Delta y\partial\Delta z}. \tag{3.28}$$

The received power in the antenna element due to the signal transmitted by the source is given by

$$P_R(\Delta x, \Delta y, \Delta z) = \left(\frac{\lambda}{4\pi d}\right)^2 G_R(\Delta x, \Delta y, \Delta z)P_T \approx |h(\Delta x, \Delta y, \Delta z)|^2 P_T, \tag{3.29}$$

with $G_R(x, y) \leq G_M$. Note also that this approximation is based on the so-called Fresnel approximation, where amplitude variations of the local channel coefficient (see equation (3.23)) over each antenna are neglected [66].

3.3.2 SIMO

Let us shift the studies focus to an ELAA with multiple outputs, where the number of outputs is much greater than one (i.e., $N \gg 1$). In the next context, equation (3.21) will be used as a frame of reference to define the characteristics of each antenna channel and the attainable array gain. In this part of the chapter, it is assumed the ELAA scenario described in figure 3.4, along with the given relative positions between antennas in the array and user. It is also assumed that, for modeling purposes, the transmitting or receiving user

(irrelevant due to reciprocity) is free to roam the XY plain. The antenna centers are still defined as $\underline{p_n}$, where n indicates the index of the said element. Similarly, the user or source is displayed as $\underline{p_s} = (x_s, y_s, z_s)$ and the receiving point as $\underline{p_r} = (x_r, y_r, z_r)$. Hence, the coupling coefficient between a user and a receive point in the ELAA is

$$c(\Delta x, \Delta y, \Delta z) = \frac{\left(\left((x_r - x_s)^2 + (y_r - y_s)^2\right)(x_r - x_s)\right)^{\frac{1}{2}}}{\sqrt{4\pi}\left((x_r - x_s)^2 + (y_r - y_s)^2 + (z_r - z_s)^2\right)^{\frac{5}{4}}} e^{-jk\left((x_r-x_s)^2+(y_r-y_s)^2+(z_r-z_s)^2\right)^{\frac{1}{2}}}. \tag{3.30}$$

The receiving points will rest on the face of the YZ plane, hence $\underline{p_r} = (0, y_r, z_r)$ and in a similar manner the transmitter or source, $\underline{p_s} = (x_s, y_s, 0)$ is displayed on the XY plane with $z_s = 0$, like displayed in figure 3.4. This way, we can iterate over all the receiving antennas in the ELAA, and as a result, the coupling coefficient becomes solely dependent on the variables x_s, Δy, and z_r. This allows us to simplify the previous equation as the following

$$c(x_s, y_s - y_r, z_r) = \frac{\left(\left(x_s^2 + (y_s - y_r)^2\right)x_s\right)^{\frac{1}{2}}}{\sqrt{4\pi}\left(x_s^2 + (y_s - y_r)^2 + z_r^2\right)^{\frac{5}{4}}} e^{-jk\left(x_s^2+(y_s-y_r)^2+z_r^2\right)^{\frac{1}{2}}}. \tag{3.31}$$

The channel response between the user and the nth antenna of the ELAA (which spans the region $\mathcal{A}_n = \{(y_r, z_r) : y_n - \frac{L}{2} \leq y_r \leq y_n + \frac{L}{2}, z_n - \frac{L}{2} \leq z_r \leq z_n + \frac{L}{2}\}$) is

$$h_n(x_s, y_s) = \sqrt{\frac{1}{A}} \int_{y_n - L/2}^{y_n + L/2} \int_{z_n - L/2}^{z_n + L/2} c(x_s, y_s - y_r, z_r) \partial y_r \partial z_r. \tag{3.32}$$

The channel gain is given by

$$|h_n(x_s, y_s)|^2 = \left| \sqrt{\frac{1}{A}} \int_{y_n - L/2}^{y_n + L/2} \int_{z_n - L/2}^{z_n + L/2} c(x_s, y_s - y_r, z_r) \partial y_r \partial z_r \right|^2. \tag{3.33}$$

The Cauchy–Bunyakovsky–Schwarz inequality states that if and only if vectors **a** and **b** are linearly dependent, the absolute value of their dot product is less than or equal to the product of their magnitudes. By considering this theorem, an upper bound on the total gain can be defined, i.e.,

$$|h_n(x_s, y_s)|^2 \leq \int_{y_n - L/2}^{y_n + L/2} \int_{z_n - L/2}^{z_n + L/2} |c(x_s, y_s - y_r, z_r)|^2 \partial y_r \partial z_r. \tag{3.34}$$

By expanding the preceding equation, we obtain

$$|h_n(x_s, y_s)|^2 \leq \int_{y_n - L/2}^{y_n + L/2} \int_{z_n - L/2}^{z_n + L/2} \frac{1}{4\pi} \frac{\left(x_s^2 + (y_s - y_r)^2\right)x_s}{(x_s^2 + (y_s - y_r)^2 + z_r^2)^{5/2}} \partial y_r \partial z_r. \tag{3.35}$$

Additionally, it is possible to specify the role of each component in the channel gain [59]. To clarify this, we can write

$$|h_n(x_s, y_s)|^2 \leq \int_{y_n-L/2}^{y_n+L/2} \int_{z_n-L/2}^{z_n+L/2} \underbrace{\frac{x_s}{\sqrt{x_s^2 + (y_s - y_r)^2 + z_r^2}}}_{\text{Directivity (T)}} \times \tag{3.36}$$

$$\underbrace{\frac{x_s^2 + (y_s - y_r)^2}{x_s^2 + (y_s - y_r)^2 + z_r^2}}_{\text{Polarization (P)}} \times \underbrace{\frac{1}{4\pi(x_s^2 + (y_s - y_r)^2 + z_r^2)}}_{\text{Pathloss (L)}} \partial y_r \partial z_r. \tag{3.37}$$

Directivity refers to the power concentration in a specific direction at a set distance from a transmitting antenna, in contrast to the power distribution equally dispersed in all directions. It is optimal to design our system with the maximum directivity value in mind to minimize losses due to the reduction of the effective area [67]. Hence, directivity functions as a quantification of the amplified maximum power focus at a specific distance compared to what is emitted by an ideal isotropic antenna. While this definition primarily pertains to transmitting antennas, it also holds true for receiving antenna due to reciprocity [67]. Given equation (3.36), the impact of the direction of arrival in the gain can be computed by

$$T = \frac{x_s}{\sqrt{x_s^2 + (y_s - y_r)^2 + z_r^2}}. \tag{3.38}$$

Taking into account a receiving element $\underline{p_n}$, located directly in front of the source of the impinging electric field, along the X axis, the directivity component of the channel gain of that specific antenna will have a unitary value. This happens because the effective area loss felt in the central antenna will be null as Δy and Δz are also zero.

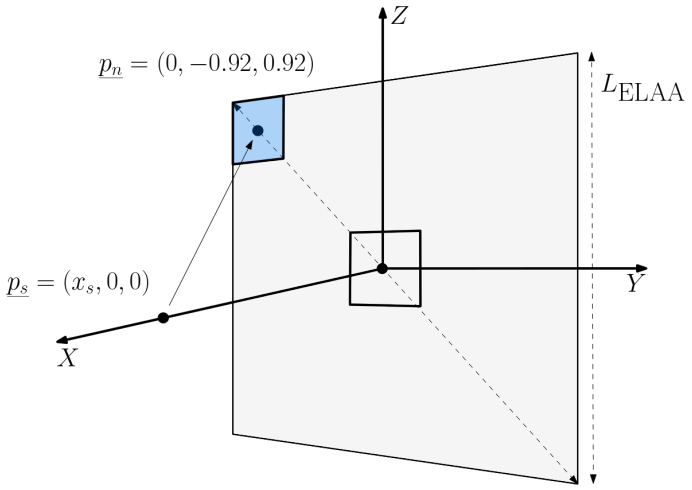

Figure 3.7: Depicted scenario.

To observe the behavior of this component of the channel gain, a comparison shall be made between the directivity impact in the near field and in the far field of a hypothetical

non-central element. For this example it is considered $\underline{p_n} = (0, -0.92, 0.92)$. This is not an arbitrary position, as it pertains to the first position of an array with $N = 11025$. Furthermore, in order to assess the distances in the near and far fields, specific values were picked. The evaluation distance in the near field is denoted as $d_{FA}/30 = 4.59m$. On the other hand, the corresponding value for the far field distance is $d_{FA} = 137.8125m$. When calculated, the impact on directivity in the far field was almost null, however in the near field, despite being small it is not negligible. This happens because for both examples the y and z components are relatively small and $d_{FA} \gg d_{FA}/30$, hence x_s has a way bigger influence in the far field.

$$T = \frac{d_{FA}}{\sqrt{d_{FA}^2 + (y_s - y_r)^2 + z_r^2}} \approx 1 \quad (3.39) \qquad T = \frac{\frac{d_{FA}}{30}}{\sqrt{\frac{d_{FA}}{30}^2 + (y_s - y_r)^2 + z_r^2}} = 0.962 \quad (3.40)$$

It is evident that as one approaches the array system, the influence of the effective area loss resulting from directivity intensifies. Another factor that contributes to the channel gain are the losses experienced in transmission due to polarization misalignments. Typically, the polarization of an antenna aligns with the direction of current flow and the current density vector within its structure. In this scenario we are, once again, using an array of aperture antenna and an isotropic radiator, they happen to be polarized in the direction of the Z axis. It is worth emphasizing that the polarization of an antenna can be influenced by its orientation in relation to the receiving antenna or the polarization of the incoming wave. When the receiving antenna deviates from the polarization of the incoming wave, a polarization mismatch may occur, leading to a decrease in signal strength. From equation (3.36), we can take the factor that equates to the polarization loss of each element, due to the deviation of polarization, given the short distance and relative size of the array in question. This factor is given by

$$P = \frac{x_s^2 + (y_s - y_r)^2}{x_s^2 + (y_s - y_r)^2 + z_r^2}. \quad (3.41)$$

Given the conditions in the previous example, we can also reach the polarization loss factor for a receiver in a non-central position and compare the influence propagation distance has on it. Considering the same $\underline{p_n}$, the loss due to polarization felt in a receiver in a central position in the YZ plane is once again null. Nevertheless, when considering a non-central receiver, such as $\underline{p_n} = (0, -0.92, 0.92)$, the polarization factor at the far field and near field is given by

$$P = \frac{d_{FA}^2 + (y_s - y_r)^2}{d_{FA}^2 + (y_s - y_r)^2 + z_r^2} \approx 1 \quad (3.42) \qquad P = \frac{\frac{d_{FA}}{30}^2 + (y_s - y_r)^2}{\frac{d_{FA}}{30}^2 + (y_s - y_r)^2 + z_r^2} = 0.963 \quad (3.43)$$

The polarization factor, like the directivity factor, is enhanced by the smaller x_s gets. This effect will also only be noticeable if we are not aligned with the central antenna. The impact on polarization increases as the difference between the norm components of the elements in the YZ plane and the user becomes larger. In other words, when there is a significant disparity between these components, it has a more pronounced effect on polarization. In equation (3.36), the factor pertaining to free-space pathloss is given by the following expression

$$L = \frac{1}{4\pi(x_s^2 + (y_s - y_r)^2 + z_r^2)}. \tag{3.44}$$

As previously mentioned, when operating in the near field region, it is essential to take into account the curvature of the incoming wave and incorporate the individual effective area, path loss, and polarization loss of each antenna element in the channel responses [63]. This stands in contrast to the conventional plane wave regime, where variations in effective area and polarization losses are disregarded, and channels are typically modeled using simplified Friis' formulas [63], [64]. Hence, equation (3.44) should seem familiar, as it is the representation of only the pathloss component in the channel gain - It pertains to the Friis formula. To further explain this concept, let us consider the effective channel over the receive region $\mathcal{A}_n$, which is the surface area occupied by the nth antenna element p_n, $\mathcal{A}_n = \{(y_r, z_r) : y_n - \frac{L}{2} \leq y_r \leq y_n + \frac{L}{2}, z_n - \frac{L}{2} \leq z_r \leq z_n + \frac{L}{2}\}$. The derived formula in equation (3.25) for received power, provides a rigorous alternative to the conventional simplified Friis' formulas, which does not neglect wave curvature at closer distances. Now, if we take the full expression pertaining to the channel gain and expand it, we get equation (3.32). Note that if the communication is happening in a region where Δx is substantially smaller than Δy and Δz to the point that we could even consider that $\mathbf{d} = \mathbf{r} - \mathbf{s} = (x_r - x_s)\hat{\mathbf{e}}_x + (y_r - y_s)\hat{\mathbf{e}}_y + (z_r - z_s)\hat{\mathbf{e}}_z = \Delta x\hat{\mathbf{e}}_x + \Delta y\hat{\mathbf{e}}_y + \Delta z\hat{\mathbf{e}}_z \approx \Delta x\hat{\mathbf{e}}_x = x_s\hat{\mathbf{e}}_x$, we obtain the following approximation for the effective channel

$$\begin{aligned}
h_n(x_s) &= \sqrt{\frac{1}{A}} \int_{\mathcal{A}_n} \frac{1}{\sqrt{4\pi}} \frac{x_s^{3/2}}{x_s^{10/4}} e^{-\mathrm{j}kx_s} \partial y_r \partial z_r \\
&= \sqrt{\frac{1}{A}} \int_{\mathcal{A}_n} \frac{1}{\sqrt{4\pi}} \frac{1}{x_s} e^{-\mathrm{j}kx_s} \partial y_r \partial z_r \\
&= \sqrt{\frac{1}{A}} \frac{1}{\sqrt{4\pi}} \frac{1}{x_s} e^{-\mathrm{j}kx_s} \int_{\mathcal{A}_n} 1 \partial y_r \partial z_r \\
&= \frac{e^{-\mathrm{j}kx_s}}{\sqrt{A4\pi}x_s} \int_{\mathcal{A}_n} 1 \partial y_r \partial z_r.
\end{aligned} \tag{3.45}$$

This scenario is equivalent to the perpendicular plane wave in the far field. Now, let us proceed with the formulation of the channel gain expression

$$
\begin{aligned}
|h_n(x_s)|^2 &= \left(\frac{1}{\sqrt{A4\pi}x_s}A\right)^2 \\
&= \frac{A}{4\pi x_s} \\
&= \left(\frac{\lambda}{4\pi x_s}\right)^2 G.
\end{aligned} \tag{3.46}
$$

Finally, these conditions lead to the simplified version of the Friis formula, which is analogous to the component of channel gain extracted in equation (3.44), as it is mostly pathloss in the far field

$$
P_R(x_s) = \frac{A_T A_R}{\lambda^2 x_s^2} P_T = \left(\frac{\frac{\lambda^2}{4\pi}}{\lambda x_s}\right)^2 G_T G_R P_T = \left(\frac{\lambda}{4\pi x_s}\right)^2 G_T G_R P_T = |h(x_s)|^2 P_T. \tag{3.47}
$$

It is also possible to investigate the same scenario imposed on the previous factor of channel gain by comparing the pathloss at a distance of d_{FA} and $d_{FA}/30$. At $d_{FA}/30$, $y_s - y_r$ and z_r will have a more significant impact on the free-space pathloss factor than at d_{FA}, such that

$$
L = \frac{1}{4\pi(d_{FA}^2 + (y_s - y_r)^2 + z_r^2)} = 5.3 \times 10^{-5} \tag{3.48}
$$

$$
L = \frac{1}{4\pi(\frac{d_{FA}}{30}^2 + (y_s - y_r)^2 + z_r^2)} = 4.4 \times 10^{-2} \tag{3.49}
$$

We define the $N \times 1$ column vector $\mathbf{h}(x_s, y_s) = [h_1(x_s, y_s)\ h_2(x_s, y_s)\ \ldots\ h_N(x_s, y_s)]^T$, as a vector composed by all channel responses between the ELAA and a user located at (x_s, y_s), where $h_n(x_s, y_s)$ is computed as in equation (3.33). On the other hand, the array gain can be computed as

$$
G_R(x_s, y_s) = \frac{\sum_{n=1}^{N} \left| \int_{\mathcal{A}_n} c(x_s, y_s - y_r, z_r) \partial y_r \partial z_r \right|^2}{\frac{\lambda^2}{4\pi} \int_{\mathcal{A}_c} |c(x_s, y_s - y_r, z_r)|^2 \, \partial y_r \partial z_r}, \tag{3.50}
$$

where $\mathcal{A}_c = \{(0, y_r, z_r) : -\frac{L}{2} \leq y_r \leq \frac{L}{2}, -\frac{L}{2} \leq z_r \leq \frac{L}{2}\}$ is the region occupied by the center antenna and c is the center antenna index given by equation (3.9). We can normalize the previous expression similarly to equation (3.28), the normalized antenna array gain can be defined as

$$
\bar{G}(x_s, y_s) = \frac{\sum_{n=1}^{N} \left| \int_{\mathcal{A}_n} c(x_s, y_s - y_r, z_r) \partial y_r \partial z_r \right|^2}{NA \int_{\mathcal{A}_c} |c(x_s, y_s - y_r, z_r)|^2 \, \partial y_r \partial z_r}. \tag{3.51}
$$

The received power in the ELAA due to the signal transmitted by the user at (x_s, y_s) is hence

$$P_R(x_s, y_s) = \left(\frac{\lambda}{4\pi d}\right)^2 G_T G_R(x_s, y_s) P_T \approx \sum_{n=1}^{N} |h_n(x_s, y_s)|^2 P_T. \tag{3.52}$$

3.4 Spatial Signal Processing

Spatial signal processing techniques can be used to improve the performance of wireless communications based on multiple antennas. It involves processing the data to be transmitted before it is sent over the wireless channel to mitigate the effects of interference and other impairments that can degrade the quality of the signal.

Generally, precoding is a generalization of beamforming in multi-antenna systems. Single-stream beamforming focuses on transmitting the same signal from each antenna at the transmitter while adjusting the phase of each signal to maximize the signal gain at the receiver output.

In order to obtain that maximum value of the transmission we will have to perform Matched Filtering (MF) beamforming. This technique assumes that the user's location is accurately known and that the communication path between the transmitter and receiver is completely clear [68]. Matched filtering beamforming, which combines the principles of matched filtering with beamforming techniques, extends these advantages to array antenna systems. By appropriately weighting the elements of an antenna array and applying matched filtering to the received signals, it becomes possible to steer the array's radiation pattern towards the desired signal direction, while minimizing interference and noise from other directions [68], [69]. Overall, matched filtering is a fundamental and powerful technique that significantly improves the signal-to-noise ratio and enhances the ability to recognize and extract desired signals, making it invaluable in a wide range of applications.

When users are in the far field, conventional Angle-of-Arrival (AoA) beamforming can be used. However, if the users are in the near field, the beamforming design should account for the spherical wave curvature, hence involving a given target position rather than a target AoA. Let us now consider the focus position as $\underline{p_F} = (x_F, y_F, 0)$. The beamforming weights for the N antennas that assure the focus on this position are defined as follows

$$\mathbf{w}(x_F, y_F) = \hat{\mathbf{h}}(x_F, y_F) = \frac{\mathbf{h}(x_F, y_F)}{||\mathbf{h}(x_F, y_F)||}. \tag{3.53}$$

The beamforming weights as presented in $\mathbf{w}(x_F, y_F)$, represent only the phase experienced by the channel response at $\underline{p_F}$. By design, we know that $||\mathbf{w}(x_F, y_F)||^2 = 1$.

The SNR is a measure of the quality of a signal relative to the background noise present in a communication system. It quantifies the ratio of the power of the signal of interest to the power of the noise. The SNR at the user is directly influenced by the

power of the signal received and inversely affected by the power of the noise present in the communication system. It is important to maintain a high SNR to ensure reliable and accurate communication, especially in scenarios where data rates are high or the communication environment is challenging. The power gain at a given position (x, y) when the focal point is $\underline{p_F}$ is given by

$$\kappa(x, y) = |\mathbf{w}_F^H \mathbf{h}(x, y)|^2. \tag{3.54}$$

Clearly, the relative maximum value is obtained at the focal point $\underline{p_F}$ since

$$\kappa(x_F, y_F) = |\mathbf{h}(x_F, y_F)|^2. \tag{3.55}$$

However, it should be highlighted that this power gain might not value not correspond to the absolute maximum. This can occur if $\underline{p_F}$ is situated in the near field region of the antenna system. We can normalize the power gain based on this perpendicular far field attainable gain so as to be coherent to the term of comparison that is the far field gain, hence it can be defined as

$$\kappa_M = \text{Max}[\kappa(x, y)], \tag{3.56}$$

where the index "M" stands as "maximum" as it represents the maximum attainable gain in a given direction, spanning from the center of the central antenna passing by $\underline{p_F}$ and landing in the far field. Under these conditions, the normalized power gain is defined as

$$\bar{\kappa}(x, y) = \frac{\kappa(x, y)}{\kappa_M} = \frac{|\hat{\mathbf{h}}(x_F, y_F)^H \mathbf{h}(x, y)|^2}{\kappa_M}. \tag{3.57}$$

Figure 3.8 illustrates the spatial arrangement of the considered locations.

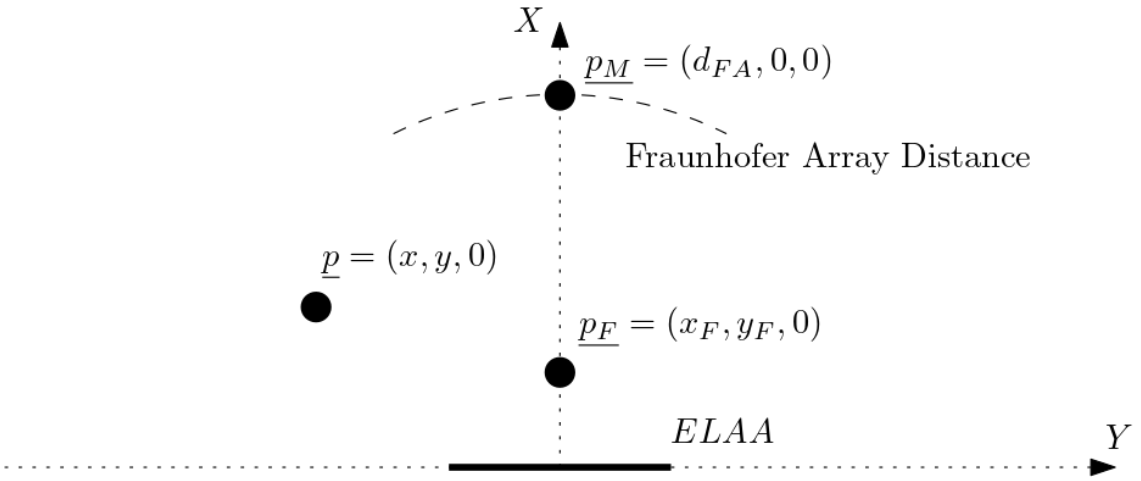

Figure 3.8: Definition of the aforementioned points in space.

This leads to the final equation for the normalized power gain, which is what we are going to study in the following sections.

In the following section, it will be considered an ELAA with $N = 105^2$ and a carrier frequency $f_c = 3GHz$, hence the wavelength would come to $\lambda = 0.10m$. Given the previous notions, it is known that $d_F = 0.0125m$ and $d_{FA} = 137.8m \approx Nd_F$.

The objective is to examine the impact of the MF on the beam depth in the near field. The initial illustrations will function as a baseline and provide a benchmark for the potential ELAA gain, notice that this gain is normalized for the maximum achievable gain.

In figure 3.9, the examination focuses on the maximum achievable gain for various distances from the infinitely extending array. It is worth noting that a unitary normalized array gain is achieved at approximately $x_F \approx d_{FA}/10 \approx 10^3 d_F$.

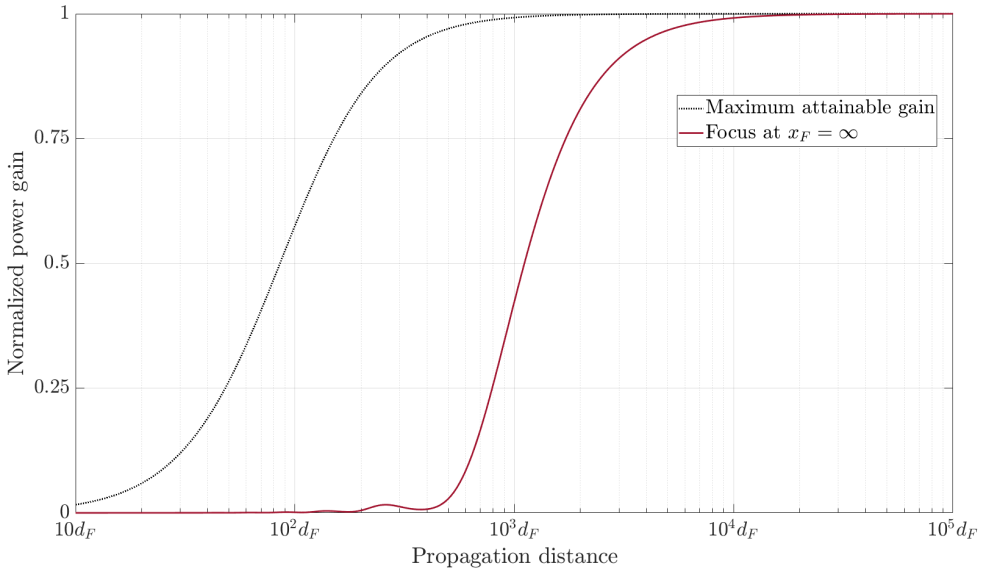

Figure 3.9: Normalized array gain when the focus is at infinity.

However, it is also important to recognize that surpassing this region as a focal point does not imply an inability to achieve further advantages, as subsequent figures will demonstrate. The red line indicator represents the normalized array gain for a focus situated at infinity or a significantly large relative Δx compared to the other distance components, namely Δy and Δz.

When the MF is parameterized as such that the focus is on $x_F = d_{FA}$, we also get an infinite beam depth as demonstrated in figure 3.10.

This is to be expected as the d_{FA} is the limit for the near field of the array. Figure 3.10 shows the array gain for a focal point in the limit of d_{FA}. The beam depth is also infinite as the MF focus is on the array's limit of the near field range.

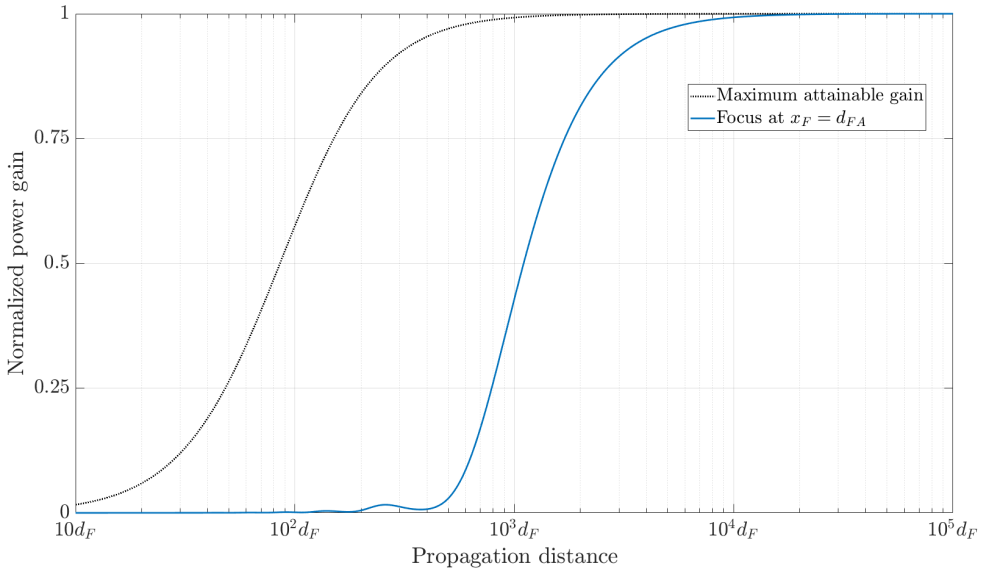

Figure 3.10: Normalized array gain when the focus is at d_{FA}.

Figure 3.11 will provide substantial context regarding the achievable gain and its behavior in the near field. Unlike the previous scenarios in which the focus was positioned beyond the far field, the following figure will illustrate the characteristics of the normalized array gain and beam depth when the MF is parameterized to place the focus within the near field region of the array.

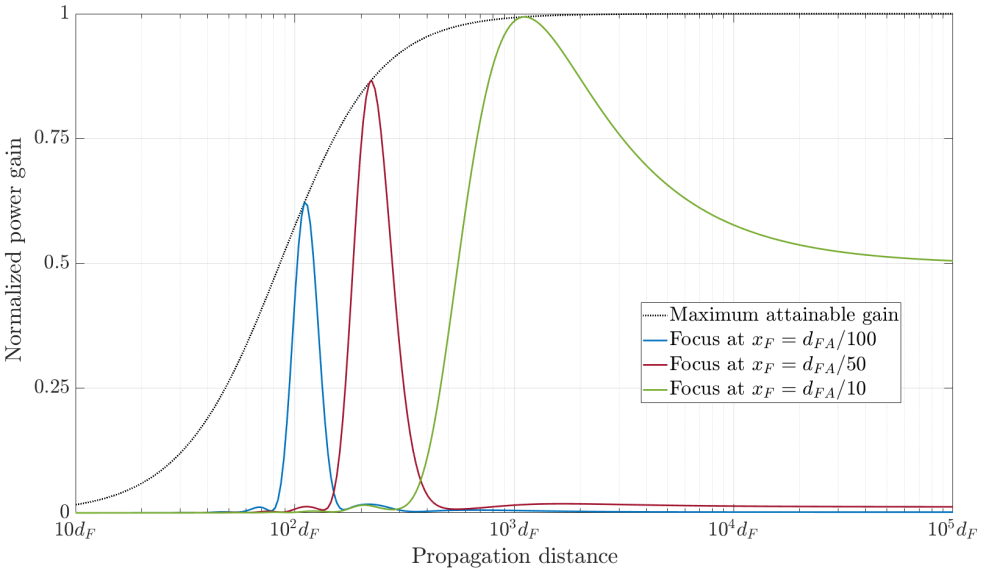

Figure 3.11: Normalized array gain when the focus is at $d_{FA}/10$, $d_{FA}/50$ and $d_{FA}/100$.

This figure holds significant importance within this section as it encompasses the

essence of the previous efforts aimed at uncovering the ideal channel model capable of incorporating the near-field phase shift and wave curvature attributes. With the aid of this comprehensive channel model and the resulting normalized power gain, it is noted that depending on the focus distance, a finite depth of focus can be achieved. For instance, at $x_F = d_{FA}/10$. This distance holds a distinct characteristic in that, despite achieving a near maximum array gain as previously observed when the MF was parameterized to focus on $x_F = d_{FA}$, a unitary normalized array gain extending infinitely is not attained. Instead, a steady decrease in array gain is experienced until reaching a plateau where the array gain equals $\bar{\kappa} = 0.5$. Let us examine another distinct focal distance characterized by the parameterization of the MF such that $x_F = d_{FA}/50$. In this case, the attainment of a unitary normalized gain is no longer observed, which aligns with expectations. As depicted in the figure, decreasing the relative distance between the array and the user results in losses in gain due to the reduction in effective area and polarization misalignments. However, it can be noted a focusing effect around $x_F = d_{FA}/50$. More concretely, it can be seen that a focal point at $x_F = d_{FA}/50$ already achieves a finite beam depth and the normalized gain is approximately zero as the distance beyond the focal point increases $\bar{\kappa} \approx 0$, which was not observed when the focal point is $x_F = d_{FA}/10$. As can be noted in figure 3.11, when $x_F = d_{FA}/100$ it can be noted that a finite beam depth can also be achieved, despite the peak normalized gain at the focal point is less than the aforementioned focus. What makes this distance unique is that the relative focus depth is around d_F, this not only implies that the position of the user must be always known with great accuracy but it also guarantees almost complete isolation from the rest of the users in the XY plane.

Furthermore, based on previous observations of distances and spatial characteristics pertaining to the positions in space relative to the array, it can be said that the most favorable scenario from a physical layer security perspective is where the user is located at the focal point. With this configuration, the user experiences the highest achievable gain at that particular distance from the array. Whilst it is important to have a high array gain, it is also desirable to have a narrow beam depth in order to minimize the potential for interference from unauthorized users seeking to disrupt the communication.

This figure illustrates the relative gain of the array when the MF is parameterized to focus on $x_F = d_{FA}/30$. Similar to the observations made in Figure 3.11, where the focus was on $x_F = d_{FA}/50$ and $x_F = d_{FA}/100$, the existence of a finite beam depth is evident in the data. Although this depth is wider compared to the other two examples, a certain degree of isolation can still be achieved. Despite possessing a finite beam depth, it is able to reach a substantial value of nearly 94% of the maximum normalized array gain, a value typically achievable only in regions relatively close to the far field region. It is thought that this particular distance is of interest since it appears to somewhat satisfy both properties. Through these observations, a notable realization emerges, highlighting the existence of a trade-off when prioritizing security in wireless communication within the near field. As the Fraunhofer array distance is approached, the behavior of the system increasingly resembles that of the far field - Infinite beam depth and high relative array gain. Thus,

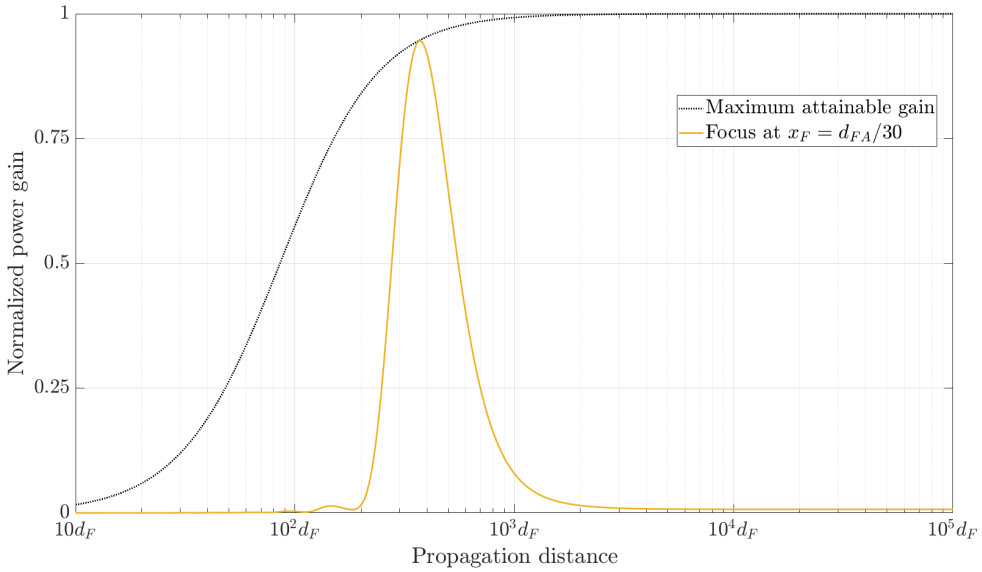

Figure 3.12: Normalized array gain when the focus is at $d_{FA}/30$.

it becomes apparent that achieving security in wireless communication within the near field necessitates careful consideration of this compromise. Like previously seen in 3.11 where $x_F = d_{FA}/10$, the normalized array gain plateaus at around 0.5, in $x_F = d_{FA}/30$, a closer distance, a finite beam depth is achieved despite the lower overall array gain.

While the aforementioned examples have provided valuable insights into the isolation of user communication based on the channel properties and the relative distance of the focal point, it is important not to rely solely on these findings. It is known that the user's position can vary across the XY plane, and therefore, the focus should be capable of narrowing down to accommodate any user position within this plane. Simply put, we should strive for a solution that can effectively narrow down the beam towards the user, regardless of their specific location in the XY plane.

In the following section, the calculation of the normalized array gain in the XY plane is presented by parameterizing the MF and thereby establishing a focus point at multiple distances relevant to the case study. This analysis serves a dual purpose: first, it facilitates a more comprehensive visualization of the insights presented in the preceding figures, and second, it provides a broader perspective on the impact of the array within the spatial vicinity of the focal point. The figures in this analysis are graphed in such a manner that the vertical axis represents a logarithmic scale for the relative position of the focus within the X axis. This logarithmic scale adheres to the same principle as the horizontal axis used in the previously presented figures. This intentional design choice ensures a sense of continuity throughout the study and enables more coherent comparisons and side-by-side representations. The horizontal axis of the figures features a linear scale representing distances in the Y axis for the beam width. This aspect holds significant

importance in the study since it considers the possibility of other users being in close proximity to the focal point, not necessarily positioned directly in front or behind it, but rather alongside it. Furthermore, to represent the value of the normalized array gain, a color map was chosen. This was done to preserve the simplicity and offer a better interpretation experience instead of a 3D figure. The highest values of the figure are also mapped using a color ruler at the right side of the picture depicting the relative value of each simulated position. Finally, for simplicity's sake, it was placed a marker on the exact spot where the focus occurs to better showcase the MF placement in the XY plane.

The initial figure illustrates the array gain behavior in the XY plane when the focus is set at $x_F = d_{FA}$. Similar to the observations made in figure 3.10, an infinite beam depth can be noted at this particular focal distance.

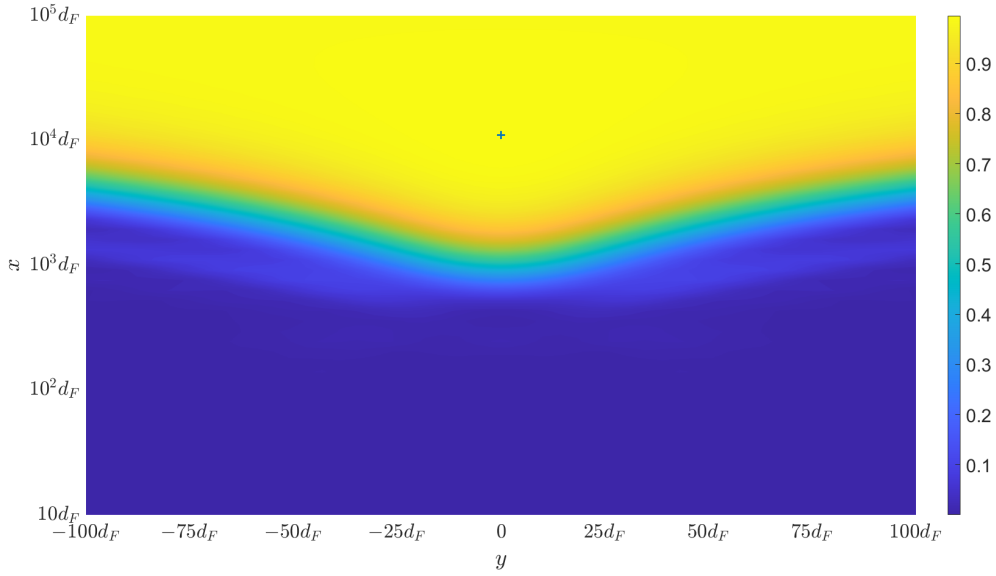

Figure 3.13: Normalized array gain for a focal point situated at the edge of the near field of the array system.

This new perspective allows us to discern that a significant portion of the space occupied by users is affected by this undesired gain, resulting in a "polluted" communication environment. Consequently, this interference can manifest as noise for other users, further emphasizing the implications of such communication dynamics.

The figure 3.14 depicts a crucial scenario wherein the focus is positioned at $x_F = d_{FA}/10$. This specific focal distance holds significant importance as it exemplifies the inherent trade-off observed in the near field. As the user moves relatively closer to the array, two key observations become apparent. Firstly, the overall normalized array gain decreases compared to the far field conditions. Secondly, while the beam depth remains infinite for $x_F = d_{FA}/10$, the array gain behind the user diminishes to half of the maximum gain experienced in the far field. These findings demonstrate the delicate balance and compromise involved in near field communications.

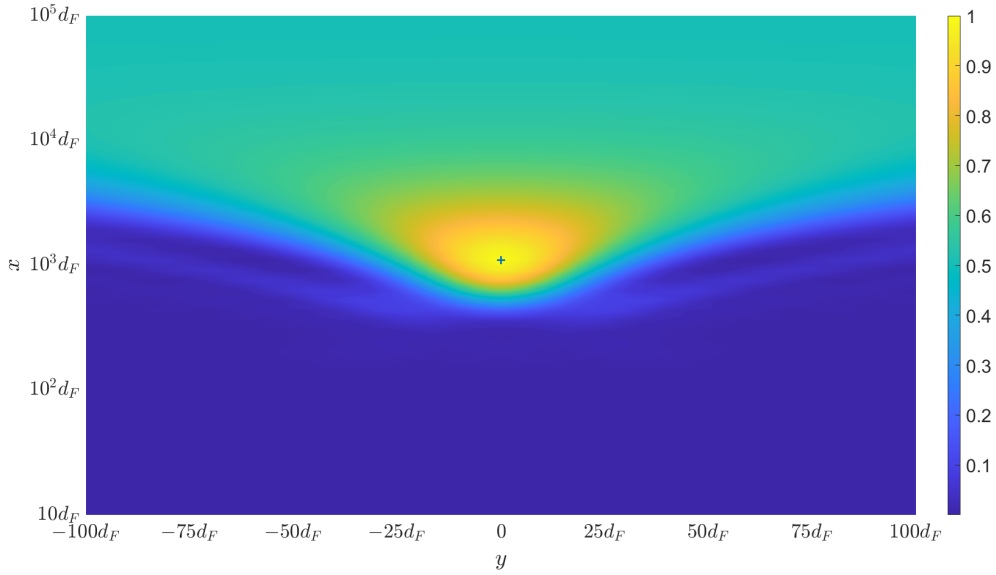

Figure 3.14: Normalized array gain for a focal point perpendicular to the array system, at $x_F = d_{FA}/10$.

The subsequent scenarios aim to demonstrate the behavior of the array gain when the focal distance reduces. Figure 3.15 also portrays the array gain in a 3D manner through a meshgrid. This depiction corresponds to the figure represented in figure 3.12.

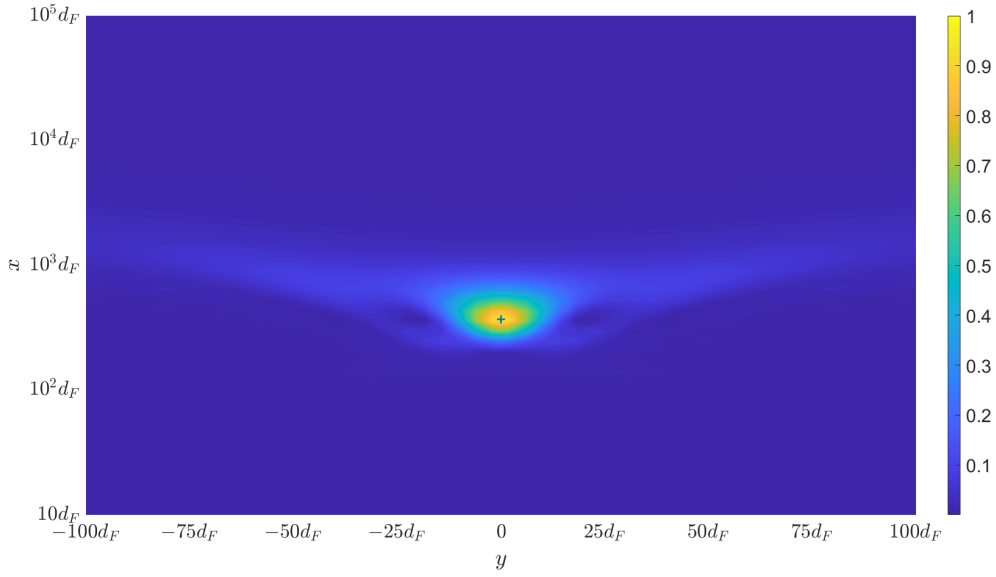

Figure 3.15: Normalized array gain for a focal point perpendicular to the array system, at $x_F = d_{FA}/30$.

From the observation, it becomes evident that not only is a relative array gain of approximately 94% achieved, but also a minimal area is influenced by the channel gain

in figure 3.15. Consequently, communication would be limited to the highlighted regions exclusively. This limited area has a width and depth of around $25d_F$, beyond which the array gain ceases to hold significance. This small area of influence leads us to the logical conclusion that communication can be effectively isolated from surrounding users. Not only would it be needed to constantly track the position of the user in question, but it would also be imperative to ensure precise coordination of transmission parameters to maintain the desired level of isolation. If these requirements were consistently met, it would be feasible to ensure a remarkably elevated level of security in communication.

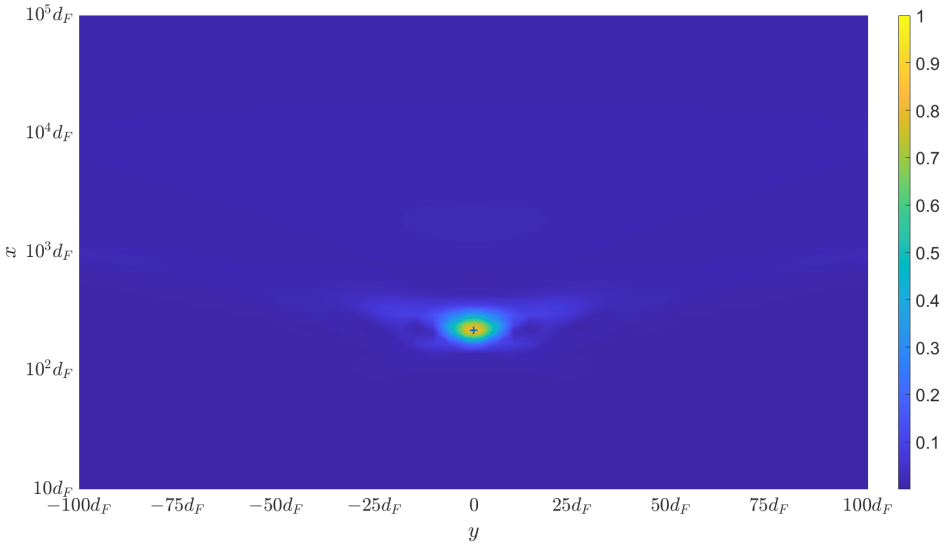

Figure 3.16: Normalized array gain for a focal point perpendicular to the array system, at $x_F = d_{FA}/50$.

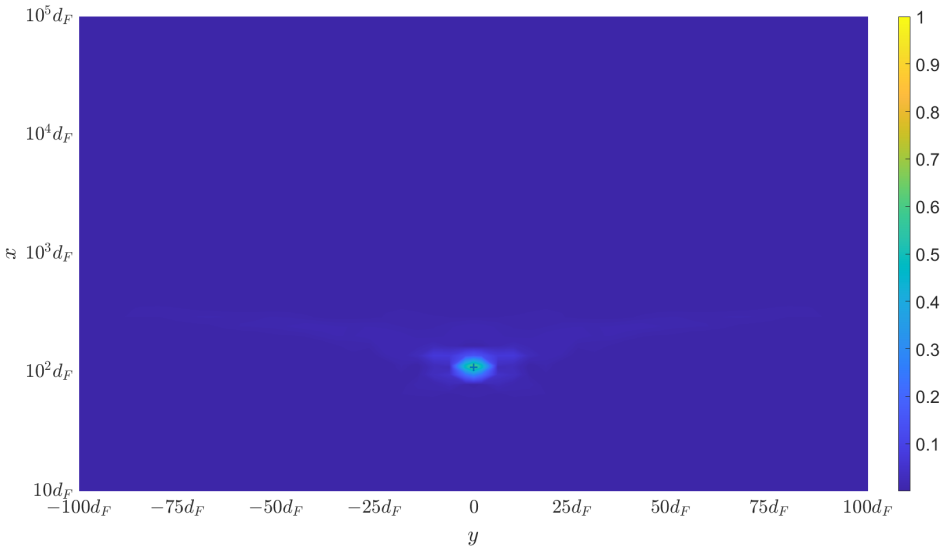

Figure 3.17: Normalized array gain for a focal point perpendicular to the array system, at $x_F = d_{FA}/100$.

All the conclusions derived from previous figures apply to figure 3.17. Of particular significance is the observation that, despite achieving an approximate 62% of the array gain experienced in the far field region of the system, we can confine the area of influence to a remarkably narrow width and depth of around $5d_F$ in figure 3.17. Comparatively, in figure 3.17 there is even less manifestation of gain in the vicinity of the focal point in the scenarios depicted in figure 3.15 and figure 3.16.

4

Physical Layer Security with near field

Based on the preceding section, it becomes apparent that near field communications possess substantial potential in achieving the objectives of PLS. When it comes to the beamforming gain at a focal point within the near field region of an ELAA, it exhibits numerous advantageous properties compared to its far field counterpart. Although the near field focal point may exhibit a lower normalized array gain, it also offers a significantly lower Depth-of-Focus (DF). As a result, communication in this context becomes much safer, as the user positioned at the focal point experiences greater isolation.

The Alice and Bob paradigm serves as a prevalent framework in the fields of cryptography and security, designed to represent distinct roles or entities within a communication scenario. Alice and Bob conventionally embody legitimate participants involved in secure communication, with one of them assuming the role of the sender or initiator, and the other as the intended recipient. In the current scenario, we interchangeably designate the role of Alice and Bob to the ELAA and the legitimate user, respectively. This interchange is done to accommodate their potential role swaps as we delve into the study of communication's downlink or uplink aspect.

Furthermore, within this scenario, we introduce two malicious entities: Eve, the eavesdropper, and Jamal the jammer. By assuming the role of an eavesdropper, Eve represents a malicious user who seeks to intercept or secretly listen to the communication exchanged between Alice and Bob, without their knowledge or authorization. Eve's primary objective is to gather unauthorized information or data. On the other hand, Jamal represents a jammer, which denotes an adversary intentionally causing disruption or interference in the communication between Alice and Bob. Jamal's malicious actions involve generating deliberate jamming signals, aiming to hinder the transmission and destroy the communication link between Alice and Bob.

In this section, we use the channel model presented in subsection 3.3 to present a study of the jamming rejection and secrecy rate of an ELAA operating in the near field and compare them to the ones observed in the far field.

By defining the position of the legitimate user as $\underline{p_l} = (x_l, y_l, 0)$, and the position of the malicious user as $\underline{p_m} = (x_m, y_m, 0)$, where $x_m = x_l + d_x$ and $y_m = y_l + d_y$, with d_x and d_y denoting the deviations relatively to $\underline{p_l}$ in the x and y directions, respectively. Since both the legitimate user and the malicious user are located in the XY plane, z_l and z_m will be equal to 0.

The distance between the legitimate user and the center of the ELAA is denoted as d_l. When users are in the far field, conventional AoA beamforming can be used. However, if the users are in the near field, the beamforming design should account for the spherical wave curvature, hence involving a given target position rather than a target AoA.

This scenario assumes that the position of legitimate and malicious users is perfectly known. This implies that the system has access to accurate location information of both users, which is crucial for designing the beamforming strategy. By utilizing the user's position, the MF can optimize the beamforming weights to maximize the signal strength at the intended user location. The beamforming weights are defined as

$$\mathbf{w}(x_l, y_l) = \hat{\mathbf{h}}(x_l, y_l) = \frac{\mathbf{h}(x_l, y_l)}{|\mathbf{h}(x_l, y_l)|}. \tag{4.1}$$

The SNR at both users depends on the beamforming gain at their position. We define the power gain at (x, y) when the focal point is $\underline{p_l}$ as

$$\kappa_l(x, y) = |\mathbf{w}(x_l, y_l)^H \mathbf{h}(x, y)|^2, \tag{4.2}$$

with the maximum value being obtained at the focal point $\underline{p_l}$ and defined as

$$\kappa_{l_M} = \kappa_l(x_l, y_l) = |\mathbf{h}(x_l, y_l)|^2. \tag{4.3}$$

On the other hand, the normalized power gain is defined as

$$\bar{\kappa_l}(x, y) = \frac{\kappa_l(x, y)}{\kappa_{l_M}}. \tag{4.4}$$

In this context, it is important to note that the normalized power gain is not scaled based on the maximum achievable gain in the specific direction of the user, as it was previously normalized using the value corresponding to the far field. The current objective is to examine the factors influencing the user's surroundings, predominantly in the near field. Due to the inherent calculation of the achievable capacity and the secrecy rate $\bar{\kappa_l}$, it consistently emerges as a fraction, with its maximum value reaching unity exclusively when $\bar{\kappa_l}(x_l, y_l)$ is considered.

Figure 4.1 shows the evolution of $\bar{\kappa_l}(x, y)$ for an ELAA with $N = 105^2 = 11025$ antennas considering a focal point $\underline{p_l}$ located in the X-axis. The normalized beamforming gain is obtained for a malicious user that can be located in a grid around $\underline{p_l}$, considering relative displacements $d_x = [10d_F, 10^5 d_F]$ and $d_y = [-50d_F, 50d_F]$. Two scenarios are shown, namely: the left focal point $\underline{p_l}$ is in the far field $x_l = d_{FA}$ and right focal point $\underline{p_l}$ is in the near field located at $x_l = d_{FA}/30$.

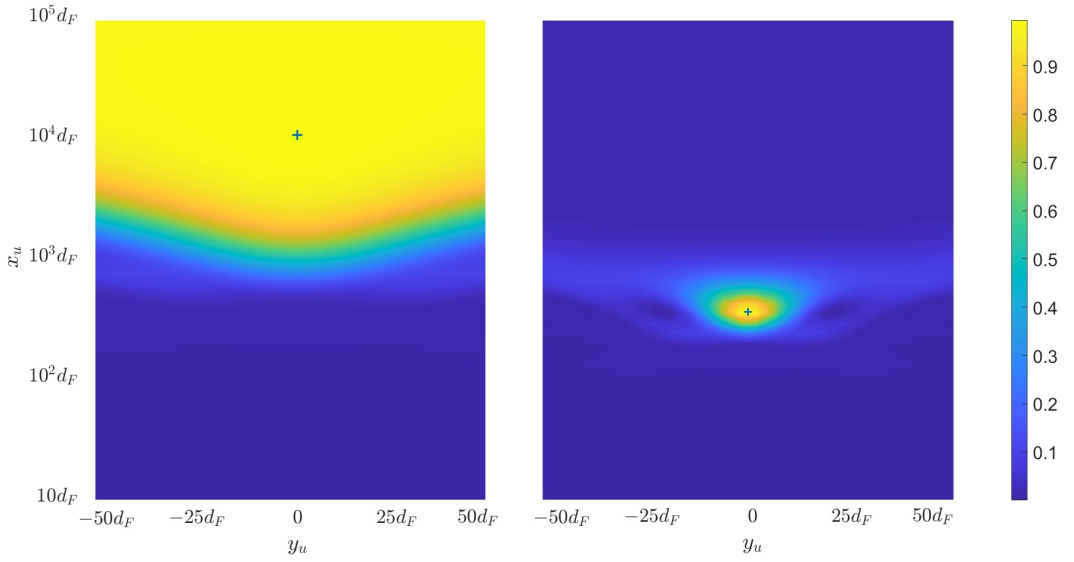

Figure 4.1: Normalized beamforming gain considering focal points: far field (left figure) and near field (right figure).

From figure 4.1, it can be observed that when the focal point is in the near field, the normalized beamforming gain around it decreases sharply with the distance at the beamforming direction, being noted that $\bar{\kappa}_l \approx 0.5$ when $d_x = 150 d_F$. This contrasts with what is observed in the far field, where $\bar{\kappa}_l$ presents large values along the beamforming direction (i.e., when $d_y = 0$). For instance, even at $x_m = x_l + 1000 d_F$, we have $\bar{\kappa}_l(x_m, y_m) \approx 0.98$.

According to [66], the Fraunhofer array distance plays a crucial role in what is called DF. If the user is situated in the far field, we can use the plane wave approximation. This allows us to determine the array response based solely on the angle of arrival or intended angle of departure and use it for MF. Meaning that all signals arriving from a said angle will be amplified. The DF of the receiving array diminishes with the distance to the transmitter. Parameterizing the MF to concentrate on a potential transmitter at a specific distance of $x_u = F$ allows us to define the DF as the distance interval ranging from F_{min} to F_{max}. Within this interval, the antenna array's gain experiences a reduction of no more than 3 dB compared to its maximum value. According to [66], this area is calculated by the following expression

$$x_u \in \left[\frac{d_{FA} F}{d_{FA} + 10F}, \frac{d_{FA} F}{d_{FA} - 10F} \right]. \tag{4.5}$$

This is only true for a focal distance that is less than $d_{FA}/10$. As 3 dB in power represents a fraction 0.5 in linear units, this is observed in figure 3.14, although in this case the upper limit is replaced by inf. Figures 4.2 and 4.3 illustrate a phenomenon previously discussed, wherein users situated at specific distances known as F_{min} and F_{max} from the focal point encounter a reduced beamforming gain, amounting to half of the total normalized gain

experienced by users precisely positioned at the center of the focal point, thus a reduction in gain of 3dB. As the focal point draws nearer to the antenna array, this range diminishes, resulting in a shorter DF and a sharper focus. Consequently, communication might become safer due to increased channel isolation. In the first figure, where the focal point is located at $d_{FA}/10$, F_{max} is infinity.

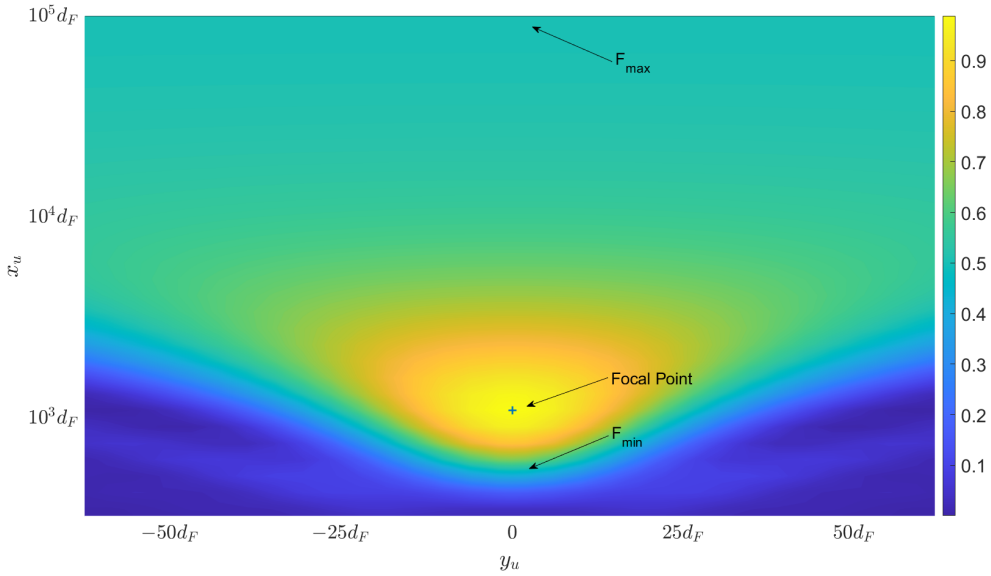

Figure 4.2: Depth of focus at $d_{FA}/10$

Figure 4.3 shows a close-up depiction of a focal point situated at $d_{FA}/30$. As can be noted, the DF is finite and much sharper.

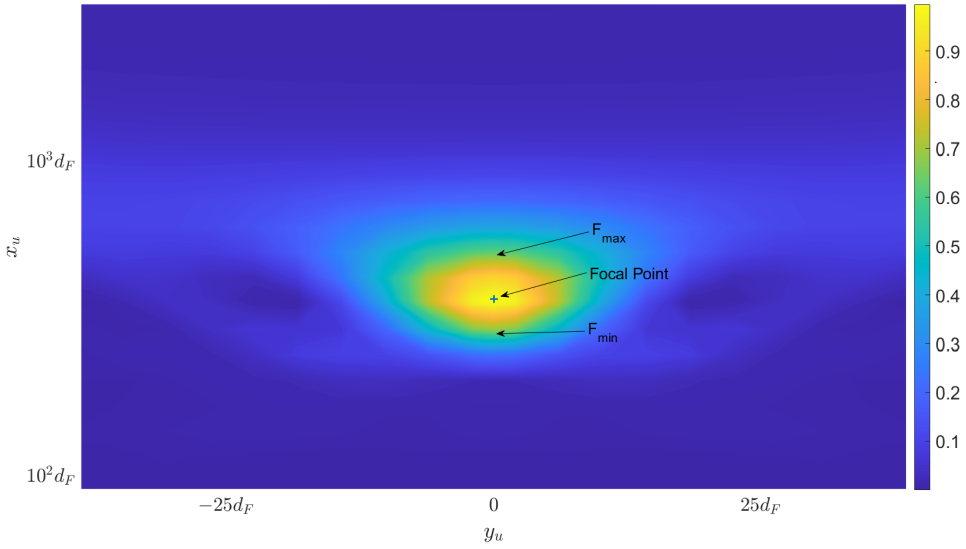

Figure 4.3: Depth of focus at $d_{FA}/30$

In the subsequent section, the notion of occupation ratio will be introduced. As

previously discussed, the value of d_{FA} is influenced by several factors, namely the operating frequency and the total number of antennas within the array. These parameters play a crucial role in determining the specific distance d_{FA} for a given system. Given this, α, the occupation ratio where $\alpha \in [0, 1]$ signifies the ratio of the total number of antenna that are being used in a given moment

$$\alpha = \frac{N_{Op}}{N}, \tag{4.6}$$

where N_{Op} is the number of operating antennas for a given α.

Figure 4.4 shows the operating array with different occupation ratios.

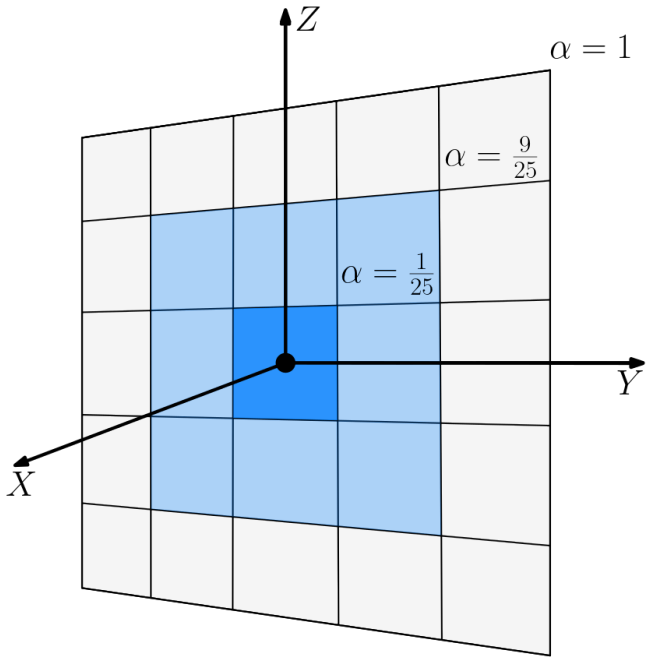

Figure 4.4: Different possible operating arrays

Hence if the total number of antenna is $N = 105^2$ and $\alpha = \frac{1}{2}$, only half of the antennas of the array are active. What this entails is the following scenario. Let's now consider a user located at the Fraunhofer array distance for an array of αN antenna, where $N = 105^2$ and $\alpha = \frac{1}{5}$. The value of d_{FA} grows as we increase the total number of antennas and if we toggle all of the elements in the array ($\alpha = 1$) the user becomes located in the near field region of the new array system.

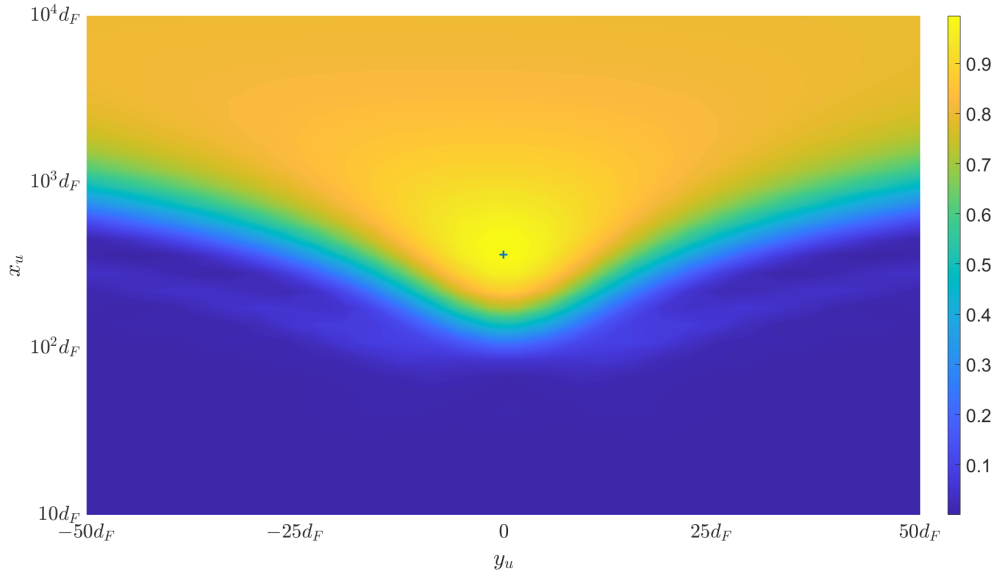

Figure 4.5: Occupation ratio of $\alpha = \frac{1}{5}$. User is fixed at the $d_{FA}/30$ for $\alpha = 1$.

Figures 4.6 and 4.5 showcases this phenomenon, as it is considered a user in a static position, and the occupation ratio of the ELAA is gradually increased. For this example, we consider $f_c = 3GHz$ as a constant.

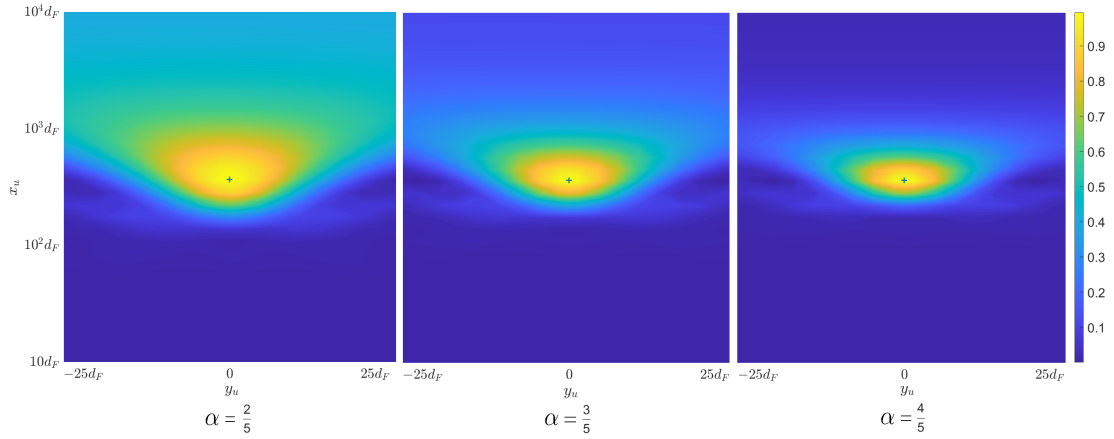

Figure 4.6: Occupation ratios of $\alpha = \frac{2}{5}$, $\alpha = \frac{3}{5}$ and $\alpha = \frac{4}{5}$ respectively. Despite the user still being fixed at the $d_{FA}/30$ for $\alpha = 1$.

The total number of antenna is $N = 105^2$. The user is located at $d_{FA}/30$ for the initial array, which is the one composed of 11025 antennas. By gradually decreasing the occupation ratio, it is noticeable that this specific point in space will migrate to the far field of the array.

Figure 4.7 depicts the user located at $d_{FA}/30$ for $\alpha = 1$ when all the antennas in the array are operating.

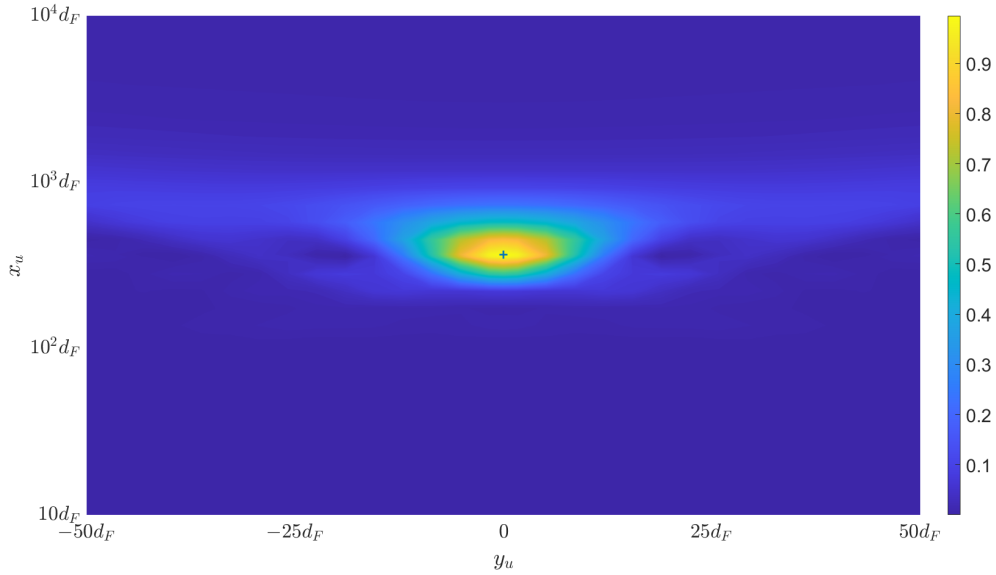

Figure 4.7: Occupation ratio of $\alpha = 1$.

Here the user experiences a maximum degree of security in communication since the DF is the smallest it can be at this distance with this number of antennas. As can be noted, when α is decreased, the gain of the array diminishes due to the utilization of a smaller number of antennas. However, this effect can be offset by increasing the power output of each individual antenna. It is important to note that our primary concern lies in addressing security issues rather than focusing on power efficiency or similar considerations.

4.1 Downlink

Let us now consider the Alice and Bob figurative scenario. Regarding the downlink, it is defined that Alice is the ELAA and is communicating with Bob, which represents the single-antenna terminal.

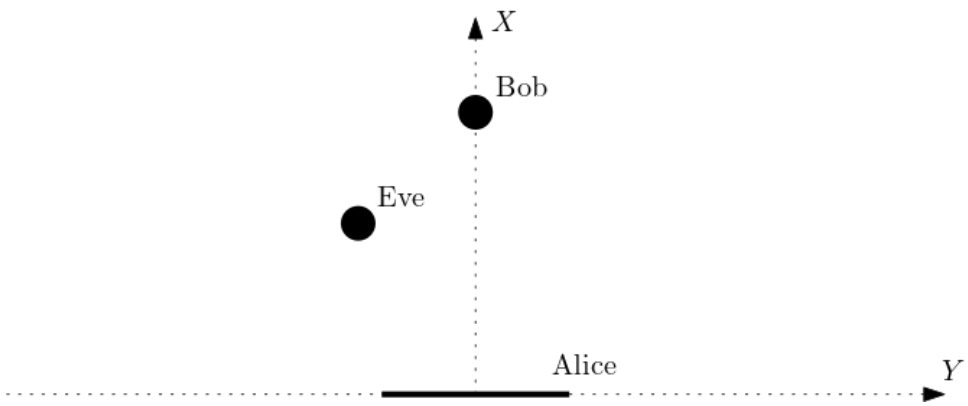

Figure 4.8: Alice, Bob and Eve displayed in the XY plane.

Meanwhile, Eve is acting as the Eavesdropper and is going to try to tap into the transmission. The goal of this subsection is to consider the ELAA PLS features to measure the secrecy rate of the communication.During the downlink transmission, the ELAA transmits a signal $s \in \mathbb{C}$ to the legitimate user with a power of P_T. The legitimate user is located at the center of the focus; therefore, according to equation (4.2), the user receives the signal as follows

$$\mathcal{Y}_l = \mathbf{h}(x_l, y_l)s + n = \sqrt{|\mathbf{h}(x_l, y_l)|^2}s + n = \sqrt{\kappa_l(x_l, y_l)}s + n = \sqrt{\kappa_{l_M}}s + n, \tag{4.7}$$

where n is the Additive White Gaussian Noise (AWGN) term and s is the transmitted signal. Here, $s \in \mathbb{C}$ and $n \sim \mathcal{CN}(0, \sigma^2)$ where the noise power is $P_N = \sigma^2$. On the other hand, the eavesdropper receives

$$\mathcal{Y}_m = \mathbf{w}(x_l, y_l)^H \mathbf{h}(x_m, y_m)s + n = \sqrt{\kappa_l}s + n. \tag{4.8}$$

By taking into account the noise power and the beamforming gain, we define the SNR in a given position as:

$$\rho_l(x, y) = |\mathbf{w}(x_l, y_l)^H \mathbf{h}(x, y)|^2 \frac{P_T}{P_N} = \kappa_l(x, y)\frac{P_T}{P_N} = \kappa_l(x, y)\rho, \tag{4.9}$$

where $\rho = \frac{P_T}{P_N}$. Here, ρ is parameterized in order to achieve 3 bps/Hz without the presence of a jammer. The maximum SNR is $\rho_{l_M} = \kappa_{l_M}\rho$, being achieved at legitimate users position. It is widely known that channel capacity associated with a given user can be calculated as a function of its SNR [70]. More specifically, the capacity associated to a user at (x, y) provided that the beamforming is designed for the focal point $\underline{p_l}$ is

$$C_l(x, y) = \log_2(1 + \rho_l(x, y)). \tag{4.10}$$

On the other hand, the eavesdropper's ability to tap the legitimate link is closely related to the secrecy rate, which is computed as the difference between the capacity of the legitimate user, $C = C_l(x_l, y_l)$, and the capacity of the eavesdropper, $C_m = C_l(x_m, y_m)$ [71], hence we get the following expression for the secrecy rate

$$\begin{aligned} S &= C - C_m, \\ &= \log_2\left(1 + \rho_{l_M}\right) - \log_2\left(1 + \rho_l(x_m, y_m)\right), \\ &= \log_2\left(1 + \kappa_{l_M}\rho\right) - \log_2\left(1 + \kappa_l(x_m, y_m)\rho\right), \\ &= \log_2\left(\frac{1 + \kappa_{l_M}\rho}{1 + \kappa_l(x_m, y_m)\rho}\right), \\ &= \log_2\left(\frac{\frac{1}{\kappa_{l_M}} + \rho}{\frac{1}{\kappa_{l_M}} + \bar{\kappa_l}\rho}\right). \end{aligned} \tag{4.11}$$

Clearly, the most unfavorable circumstance concerning data protection arises when both users are physically situated in close proximity to each other, resulting in $\bar{\kappa_l} = 1$, thereby yielding a secrecy rate of $S = 0$ bps/Hz. However, in the case of any other eavesdropper location, it can be affirmed that the secrecy rate will always remain positive.

In order to study the impact of the field region on the secrecy rate, let us consider an ELAA with $N = 105^2 = 11025$ antennas (which occupies roughly 4m^2), with a given occupation ratio α and a fixed focal point $\underline{p_l} = (x_l, y_l) = d_{FA}/30$ for $\alpha = 1$.

Figure 4.9 shows the evolution of the secrecy rate experienced by the legitimate user considering different values of α and an eavesdropper with a displacement in the range $d_x = [0, 5000 d_F]$ in the beamforming direction.

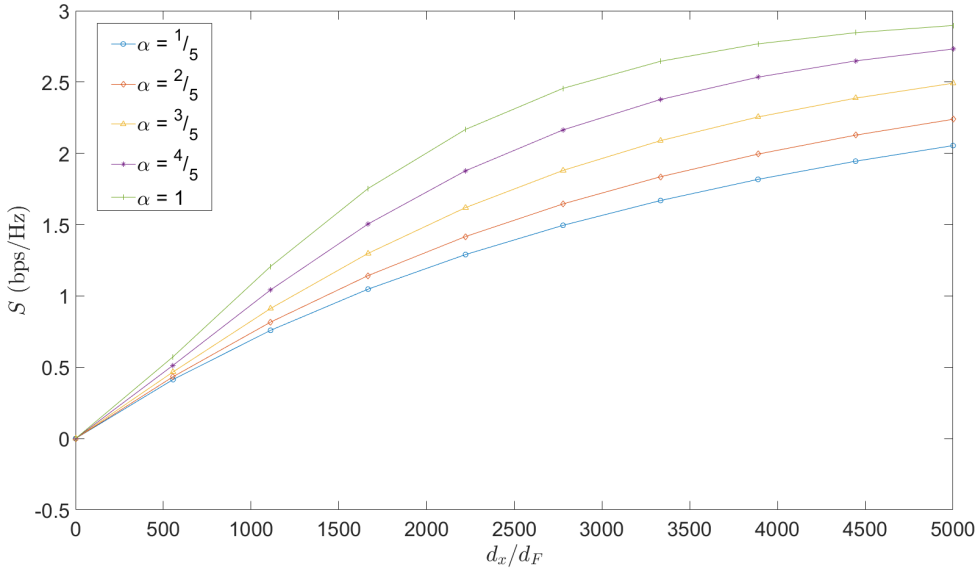

Figure 4.9: Secrecy rate considering an ELAA with different occupation ratios α.

Based on the figure 4.9, it is evident that the secrecy rate remains significantly low for small values of d_x, irrespective of α. This can be attributed to the identical beamforming gain experienced by both the legitimate user and the malicious user. Furthermore, as d_x increases, the secrecy rate S approaches its maximum attainable value (C), with C_m approximating zero. Additionally, the figure demonstrates that beyond a certain d_x value, the secrecy rate exhibits an upward trend as α increases. This can be justified by the escalating effective array size, leading to the gradual entry of the focal point into the near field as α rises.

An interesting observation is that when $\alpha = 1$, the focal point is located at $d_{FA}/30$. This particular configuration enables the beamfocusing effect and significantly degrades the SNR experienced by the eavesdropper. Consequently, such conditions contribute to an enhancement in the secrecy rate. Conversely, in situations where α deviates from 1, the focal point begins to migrate to a far field regime, resulting in a stronger signal-to-noise

ratio of the eavesdropper's communication.

This implies that the occupation ratio α can be manipulated to regulate the secrecy rate, providing a degree of freedom in terms of physical layer security. By adjusting α, one can effectively manage the beamforming properties and optimize the trade-off between achievable secrecy and system performance. This insight underscores the potential for practical applications and adaptive control mechanisms in PLS systems.

4.2 Uplink

In light of the recurring Alice and Bob analogy, let us consider the uplink scenario where Alice, functioning as the legitimate user, communicates with Bob, which is represented by the ELAA. However, in this case, the users must be wary of Jamal the jammer, which is trying and ruin their communication. This scenario is depicted in figure 4.10. Given the noise produced by Jamal, i.e., the jamming signal, the objective of this section is to presents results of the capacity of the legitimate communication link between Alice and Bob given signal-to-noise plus jamming ratio (SNJR).

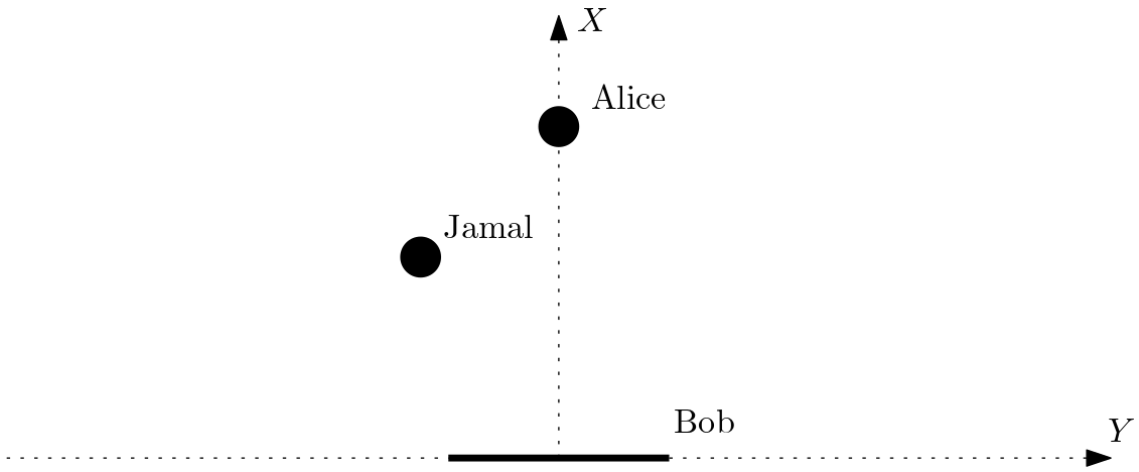

Figure 4.10: Alice, Bob and Jamal displayed in the XY plane.

Considering the uplink, the received signal at the ELAA is represented by the following expression

$$\mathcal{Y} = \mathbf{h}(x_l, y_l)s_l + \sqrt{\beta}\mathbf{h}(x_m, y_m)s_m + \boldsymbol{\nu}, \tag{4.12}$$

where s_l is the signal transmitted by the legitimate user, s_m is the jamming signal, β is a scale power factor of the jamming and ν is AWGN.

Here $\boldsymbol{\nu} \sim \mathcal{CN}(0, \sigma^2\mathbf{I}_N)$ is a vector that represents the AWGN components of the different receive antennas and $s_l \in \mathbb{C}$ and $s_m \in \mathbb{C}$ are the data symbols transmitted by the legitimate and malicious user, respectively. Hence, the combined signal after MF beamforming is given by

$$\begin{aligned}
\mathcal{Z} &= \mathbf{w}(x_l, y_l)^H \mathcal{Y}, \\
&= \mathbf{w}(x_l, y_l)^H \left(\mathbf{h}(x_l, y_l)s_u + \sqrt{\beta}\mathbf{h}x_m, y_m)s_m + \boldsymbol{\nu}\right), \\
&= \left(\mathbf{w}(x_l, y_l)^H\mathbf{h}(x_l, y_l)s_u + \sqrt{\beta}\mathbf{w}(x_l, y_l)^H\mathbf{h}x_m, y_m)s_m + \boldsymbol{\nu}\right).
\end{aligned} \tag{4.13}$$

Note that the term $\mathbf{w}(x_u, y_u)^H\boldsymbol{\nu}$ is the combined noise with power $P_N = \sigma^2$. Therefore, the transmit SNR is defined as $\rho = \frac{P_T}{P_N}$. In the presence of a jamming signal, the capacity

becomes dependent on the SNJR, which is defined as a function of the position of the jamming user $\underline{p_m} = (x_m, y_m)$ provided that the focal point is the location of legitimate user $\underline{p_l} = (x_l, y_l)$, i.e.,

$$\begin{aligned}\rho(x_m, y_m) &= \frac{\kappa_{l_M} P_T}{\beta\kappa_l(x_m, y_m) + P_N}, \\ &= \frac{\rho\kappa_{l_M}}{\beta\rho\kappa_l(x_m, y_m) + 1}, \\ &= \frac{1}{\beta\bar{\kappa_l}(x_m, y_m) + \frac{1}{\rho\kappa_{l_M}}}.\end{aligned} \tag{4.14}$$

The achievable capacity at the focal point $\underline{p_l} = (x_l, y_l)$ in the presence of a jamming signal at $\underline{p_m} = (x_m, y_m)$ is given by

$$C_l^m(x_m, y_m) = \log_2\left(1 + \frac{1}{\beta\bar{\kappa_l}(x_m, y_m) + \frac{1}{\rho_{l_M}}}\right). \tag{4.15}$$

As in the downlink case, the worst-case scenario arises when the legitimate and malicious users are co-located. To access the impact of the jamming signal, we define the normalized achievable capacity which is the ratio between the capacity with and without the jamming signal:

$$\bar{C}_l^m(x_m, y_m) = \frac{C_l^m(x_m, y_m)}{C}. \tag{4.16}$$

Similar to the previous section, we examine a scenario involving an ELAA with a total of $N = 105^2 = 11025$ antennas, a fixed focal point $\underline{p_l} = (x_l, y_l) = d_{FA}/30$ for $\alpha = 1$. Figure 4.11 shows the normalized achievable capacity considering different values of β, for an occupation ratio of $\alpha = 1$, meaning that this point is within the near field of the array. The jamming user in the beamforming direction with a relative displacement $d_x = [0, 5000d_F]$.

As can be noted from the figure, a higher value of β increases the jamming potential. When the user is in the near field, the achievable capacity rapidly increases as the jamming user moves away, which is explained by the fact that the array exhibits spatial selectivity in the beamforming direction due to a short DF.

For instance, for $d_{FA}/30$ and $\alpha = 1$, the achievable capacity at $x_m = x_l + 2500d_F$ is 88%, 79%, 65% and 30%, respectively. This observation illustrates that in the near field, the array demonstrates a notable degree of spatial selectivity in the beamforming direction, resulting in the enhanced capability to effectively mitigate the impact of the jamming signal.

In figure 4.11, it is noticeable that as the jamming user distances themselves from the system, the achievable capacity for the legitimate user in the far field exhibits a relative increase. This can be attributed to the absence of spatial selectivity in the array's beamforming direction, which leads to both users experiencing comparable levels of array gain. In fact, in far field, the normalized power gain $\bar{\kappa_l}$ is given by the ratio between the

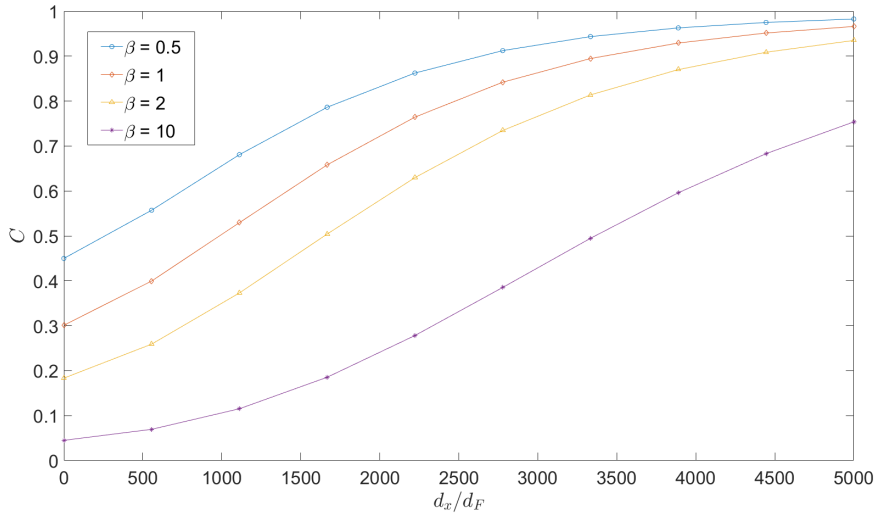

Figure 4.11: Normalized achievable capacity considering different values of β and different focal points.

X axis coordinates of the malicious and legitimate user, $\bar{\kappa_l} = \left(\frac{x_m}{x_l}\right)^2$, confirming that the beamfocusing effect is not available. However, when the legitimate user is in the near field, the jamming effect reduces substantially when the jamming user moves away from the focal point.

Figure 4.12 shows the evolution of the achievable capacity for different values of α when the jamming user in the beamforming direction, operates with $\beta = 1$ and is located with a relative displacement $d_x = [0, 5000 d_F]$.

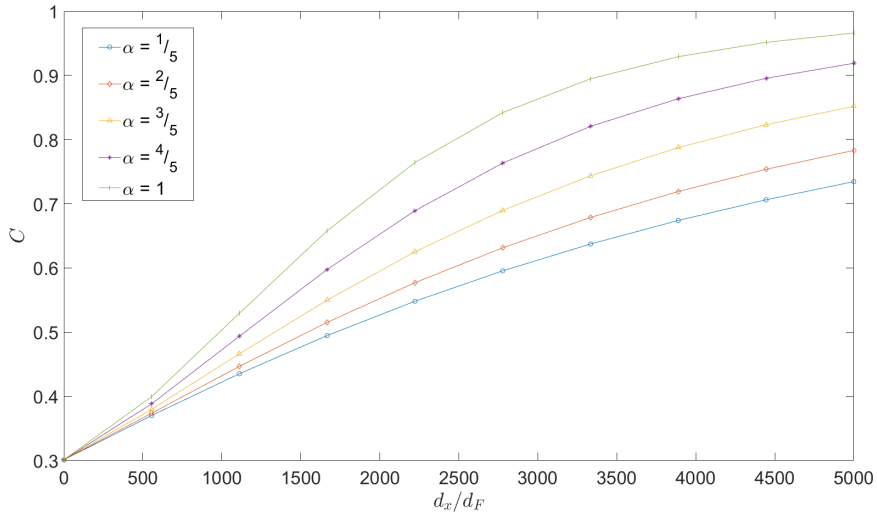

Figure 4.12: Normalized achievable capacity considering an ELAA with different occupation ratios α.

It is considered that the legitimate user is in the near field for $\alpha = 1$ with a fixed location equal to $d_{FA}/30$ and it will slowly migrate to the far field with the decrease in occupation

ratio. As anticipated, when the value of α is set to $\frac{1}{5}$, the capacity exhibits a gradual decrease as the jamming user moves away from the legitimate user, primarily due to the focal point being situated in the far field. However, as α increases and more antennas are incorporated in the communication, the effective area of the ELAA sub-array expands, resulting in an increased achievable capacity for the same displacement d_x. This can be attributed to the shifting of the focal point towards the near field, where the focusing effect becomes accessible.

As expected, the optimal performance in terms of jamming rejection occurs when α is equal to 1, employing all available antennas for beamforming. When α equals 1, the legitimate user is positioned at an effective distance of $d_{FA}/30$ from the ELAA, within the near field range where beamfocusing characteristics are applicable. This observation demonstrates that the effective ELAA employed for communication can dynamically expand or contract, based on the desired level of jamming rejection, thereby offering a notable degree of flexibility in terms of PLS.

5

Conclusions

This study involved an analysis of the telecommunications sector, with a particular focus on the utilization, capacity enhancements, and accessibility improvements associated with MIMO systems. Moreover, we introduced the concept of near-field communication and its potential for PLS, alongside the exploration of cutting-edge Extremely Large Antenna Arrays such as RIS and LIS, designed to propel future MIMO advancements. We underscored the critical importance of physical layer security and provided an overview of prevailing methodologies. The primary objective of this thesis was to expand upon these areas of investigation, encompassing the implementation of an antenna array and a meticulous analysis of the physical layer security attributes inherent to near-field beamforming.

In conclusion, our study in both the downlink and uplink scenarios has provided a comprehensive understanding of the impact of near-field beamforming on PLS and system performance. We have observed that the occupation ratio α plays a crucial role in shaping the beamforming properties, which in turn affect the secrecy rate and jamming resilience. In the downlink, we found that adjusting α allows for the optimization of secrecy rate by manipulating the beamforming gain, with a notable enhancement in secrecy achievable when the focal point is in the near field. In the uplink, we observed that varying α offers flexibility in adapting the effective antenna array size, which can be strategically expanded or contracted to improve jamming rejection.

Our comprehensive channel model, which accounts for both far-field and near-field scenarios, has enabled accurate simulations and analysis, shedding light on the intricate interplay between beamforming gains and user capacity. By considering the Friis formula approximation and wave curvature effects, we have provided valuable insights into the practical implications of near-field beamforming for enhancing security and system performance. This research offers a foundation for practical applications and adaptive control mechanisms in PLS systems, emphasizing the potential for significant advancements in the field of wireless communication security.

Despite the obtained results, this research project encountered certain limitations

that impacted the thorough investigation of the channel gain for users positioned non-perpendicularly to the array. Consequently, while it was feasible to calculate the beamforming gain for positions other than those perpendicular to the user, the study of secrecy rate and susceptibility to jamming attacks was solely conducted when a malicious user moved away from the focal point where the legitimate user was positioned. Additionally, the research scenario was limited to LoS three-dimensional space, without accounting for other multipath components that affect communication such as the ones generated by possible reflections in the propagation environment.

The exploration of physical layer security characteristics in near-field communication represents an emerging and significant topic in the field of communications. The findings shed light on the potential for utilizing the unique properties of near-field communication to enhance the security of wireless systems. By understanding and leveraging these characteristics, researchers can develop innovative techniques to mitigate eavesdropping, jamming, and other security threats. The significance of these findings lies in their potential to strengthen the confidentiality and integrity of wireless communications, paving the way for more secure and robust wireless networks in various domains.

As an example, in the realm of military and defense, leveraging physical layer security characteristics in near-field communication holds significant implications. The findings in this area offer opportunities to establish secure and reliable communication links in military applications. By utilizing near-field communication, military forces can enhance the confidentiality and integrity of sensitive information exchanged on the battlefield or during strategic operations. This technology provides a robust defense against eavesdropping, jamming, and other forms of threats, ensuring the secure transmission of mission-critical data and maintaining operational secrecy. Implementing physical layer security in near-field communication enables military personnel to communicate with utmost confidence and trust in the integrity of their communication channels, ultimately enhancing situational awareness, command and control capabilities, and the overall effectiveness of military operations.

Future research endeavors should prioritize the investigation of the physical layer security capabilities of near-field channels in scenarios where the user is positioned at varying angles relative to the studied array. It is crucial to develop comprehensive simulations that illustrate the relative distances from the focal point at which a malicious user needs to be situated to attain specific capacity levels, not just behind the user. Additionally, it is imperative to account for potential errors in tracking and beam focusing pertaining to the legitimate user. Understanding the implications of even slight localization errors on communication performance and data rates is vital. We should also be able to study further multipath components, as the adopted scenario could not account for reflections of the signals. By addressing these aspects, researchers can gain a deeper understanding of the complexities involved in near-field communication and enhance the overall security and efficiency of wireless systems.

By exploring near-field communication, physical layer security, and cutting-edge

antenna arrays, we have uncovered new insights and possibilities for advancing wireless communications. The findings underscore the significance of near-field beamforming in enhancing security and resilience against adversarial interference. This research sets the stage for future investigations into the complex dynamics of near-field channels and paves the way for innovative approaches to strengthen the confidentiality and integrity of wireless networks.

Bibliography

[1] H. Viswanathan and M. Weldon. "The past, present, and future of mobile communications". In: *Bell Labs Technical Journal* 19 (2014), pp. 8–21 (cit. on p. 6).

[2] M. A. Albreem. "5G wireless communication systems: Vision and challenges". In: *2015 International Conference on Computer, Communications, and Control Technology (I4CT)*. IEEE. 2015, pp. 493–497 (cit. on p. 6).

[3] C. Bockelmann et al. "Massive machine-type communications in 5G: Physical and MAC-layer solutions". In: *IEEE Communications Magazine* 54.9 (2016), pp. 59–65 (cit. on p. 6).

[4] H. Ji et al. "Ultra-reliable and low-latency communications in 5G downlink: Physical layer aspects". In: *IEEE Wireless Communications* 25.3 (2018), pp. 124–130 (cit. on p. 6).

[5] Y. Polyanskiy, H. V. Poor, and S. Verdú. "Channel coding rate in the finite blocklength regime". In: *IEEE Transactions on Information Theory* 56.5 (2010), pp. 2307–2359 (cit. on p. 7).

[6] H. Gamage, N. Rajatheva, and M. Latva-Aho. "Channel coding for enhanced mobile broadband communication in 5G systems". In: *2017 European conference on networks and communications (EuCNC)*. IEEE. 2017, pp. 1–6 (cit. on p. 7).

[7] J. G. Andrews et al. "What will 5G be?" In: *IEEE Journal on selected areas in communications* 32.6 (2014), pp. 1065–1082 (cit. on p. 7).

[8] K. Mallinson. "The path to 5G: as much evolution as revolution". In: *IEEE Communications Magazine* (2016) (cit. on p. 7).

[9] S. Suyama et al. "5G multi-antenna technology and experimental trials". In: *2016 IEEE International Conference on Communication Systems (ICCS)*. IEEE. 2016, pp. 1–6 (cit. on p. 7).

[10] F. Boccardi et al. "Five disruptive technology directions for 5G". In: *IEEE communications magazine* 52.2 (2014), pp. 74–80 (cit. on p. 8).

[11] M. Shafi et al. "5G: A tutorial overview of standards, trials, challenges, deployment, and practice". In: *IEEE journal on selected areas in communications* 35.6 (2017), pp. 1201–1221 (cit. on p. 8).

[12] P. Yang et al. "6G wireless communications: Vision and potential techniques". In: *IEEE network* 33.4 (2019), pp. 70–75 (cit. on pp. 8, 9, 17).

[13] A. S. Cacciapuoti et al. "Beyond 5G: THz-based medium access protocol for mobile heterogeneous networks". In: *IEEE Communications Magazine* 56.6 (2018), pp. 110–115 (cit. on p. 8).

[14] H. Yao et al. "The space-terrestrial integrated network: An overview". In: *IEEE Communications Magazine* 56.9 (2018), pp. 178–185 (cit. on p. 8).

[15] I. F. Akyildiz, C. Han, and S. Nie. "Combating the distance problem in the millimeter wave and terahertz frequency bands". In: *IEEE Communications Magazine* 56.6 (2018), pp. 102–108 (cit. on p. 9).

[16] C. Han, A. O. Bicen, and I. F. Akyildiz. "Multi-wideband waveform design for distance-adaptive wireless communications in the terahertz band". In: *IEEE Transactions on Signal Processing* 64.4 (2015), pp. 910–922 (cit. on p. 9).

[17] C. Han and I. F. Akyildiz. "Distance-aware bandwidth-adaptive resource allocation for wireless systems in the terahertz band". In: *IEEE Transactions on Terahertz Science and Technology* 6.4 (2016), pp. 541–553 (cit. on p. 9).

[18] P. Yang et al. "Multidomain index modulation for vehicular and railway communications: A survey of novel techniques". In: *ieee vehicular technology magazine* 13.3 (2018), pp. 124–134 (cit. on p. 9).

[19] M. G. Kibria et al. "Big data analytics, machine learning, and artificial intelligence in next-generation wireless networks". In: *IEEE access* 6 (2018), pp. 32328–32338 (cit. on p. 9).

[20] S. Mumtaz et al. "Terahertz communication for vehicular networks". In: *IEEE Transactions on Vehicular Technology* 66.7 (2017) (cit. on p. 9).

[21] K. Wakunami et al. "Projection-type see-through holographic three-dimensional display". In: *Nature communications* 7.1 (2016), pp. 1–7 (cit. on p. 10).

[22] M. Simsek et al. "5G-enabled tactile internet". In: *IEEE Journal on Selected Areas in Communications* 34.3 (2016), pp. 460–473 (cit. on p. 10).

[23] K. S. Kim et al. "Ultrareliable and low-latency communication techniques for tactile internet services". In: *Proceedings of the IEEE* 107.2 (2018), pp. 376–393 (cit. on p. 10).

[24] G. V. Zàruba et al. "Indoor location tracking using RSSI readings from a single Wi-Fi access point". In: *Wireless networks* 13.2 (2007), pp. 221–235 (cit. on p. 10).

[25] S. Dang et al. "What should 6G be?" In: *Nature Electronics* 3.1 (2020), pp. 20–29 (cit. on pp. 10, 11).

[26] F. Tariq et al. "A speculative study on 6G". In: *IEEE Wireless Communications* 27.4 (2020), pp. 118–125 (cit. on p. 10).

[27] S. Ullah et al. "A comprehensive survey of wireless body area networks". In: *Journal of medical systems* 36.3 (2012), pp. 1065–1094 (cit. on p. 10).

[28] H. Zhang et al. "6G Wireless Communications: From Far-field Beam Steering to Near-field Beam Focusing". In: *arXiv preprint arXiv:2203.13035* (2022) (cit. on pp. 11, 17–19).

[29] T. Javornik et al. "MIMO: Wireless Communications". In: *Encyclopedia of Wireless and Mobile Communications*. 2008 (cit. on pp. 12, 13).

[30] L. Zheng and D. N. C. Tse. "Diversity and multiplexing: A fundamental tradeoff in multiple-antenna channels". In: *IEEE Transactions on information theory* 49.5 (2003), pp. 1073–1096 (cit. on p. 12).

[31] S. N. Diggavi et al. "Great expectations: The value of spatial diversity in wireless networks". In: *Proceedings of the IEEE* 92.2 (2004), pp. 219–270 (cit. on p. 13).

[32] N. Al-Dhahir. "Single-carrier frequency-domain equalization for space-time block-coded transmissions over frequency-selective fading channels". In: *IEEE Communications Letters* 5.7 (2001), pp. 304–306 (cit. on p. 13).

[33] E. Telatar. "Capacity of multi-antenna Gaussian channels". In: *European transactions on telecommunications* 10.6 (1999), pp. 585–595 (cit. on p. 14).

[34] G. J. Foschini. "Layered space-time architecture for wireless communication in a fading environment when using multi-element antennas". In: *Bell labs technical journal* 1.2 (1996), pp. 41–59 (cit. on p. 14).

[35] B. Hassibi and B. M. Hochwald. "How much training is needed in multiple-antenna wireless links?" In: *IEEE Transactions on Information Theory* 49.4 (2003), pp. 951–963 (cit. on p. 14).

[36] L. Zheng and D. Tse. "Diversity and multiplexing: a fundamental tradeoff in multiple-antenna channels". In: *IEEE Transactions on Information Theory* 49.5 (2003), pp. 1073–1096. DOI: 10.1109/TIT.2003.810646 (cit. on pp. 14, 16).

[37] S. Coleri et al. "Channel estimation techniques based on pilot arrangement in OFDM systems". In: *IEEE Transactions on broadcasting* 48.3 (2002), pp. 223–229 (cit. on pp. 15, 16).

[38] M. Cicerone, O. Simeone, and U. Spagnolini. "Channel Estimation for MIMO-OFDM Systems by Modal Analysis/Filtering". In: *IEEE Transactions on Communications* 54.11 (2006), pp. 2062–2074. DOI: 10.1109/TCOMM.2006.884849 (cit. on p. 15).

[39] L. Lu et al. "An overview of massive MIMO: Benefits and challenges". In: *IEEE journal of selected topics in signal processing* 8.5 (2014), pp. 742–758 (cit. on pp. 15, 16, 30).

[40] O. Elijah et al. "A comprehensive survey of pilot contamination in massive MIMO—5G system". In: *IEEE Communications Surveys & Tutorials* 18.2 (2015), pp. 905–923 (cit. on p. 16).

[41] J. Lin and T. Itoh. "Active integrated antennas". In: *IEEE Transactions on Microwave Theory and Techniques* 42.12 (1994), pp. 2186–2194 (cit. on p. 17).

[42] Z. Zhang et al. "Active RIS vs. passive RIS: Which will prevail in 6G?" In: *IEEE Transactions on Communications* (2022) (cit. on pp. 17, 18).

[43] P. Nepa and A. Buffi. "Near-field-focused microwave antennas: Near-field shaping and implementation." In: *IEEE Antennas and Propagation Magazine* 59.3 (2017), pp. 42–53 (cit. on p. 18).

[44] M. Cui et al. "Near-field communications for 6G: Fundamentals, challenges, potentials, and future directions". In: *arXiv preprint arXiv:2203.16318* (2022) (cit. on pp. 19, 20).

[45] N. Decarli and D. Dardari. "Communication modes with large intelligent surfaces in the near field". In: *IEEE Access* 9 (2021), pp. 165648–165666 (cit. on p. 20).

[46] D. A. Miller. "Waves, modes, communications, and optics: a tutorial". In: *Advances in Optics and Photonics* 11.3 (2019), pp. 679–825 (cit. on p. 20).

[47] H. Zhang et al. "Beam focusing for near-field multi-user MIMO communications". In: *IEEE Transactions on Wireless Communications* (2022) (cit. on p. 20).

[48] C. S. R. Murthy and B. Manoj. *Ad hoc wireless networks: Architectures and protocols, portable documents*. Pearson education, 2004 (cit. on p. 21).

[49] Y.-S. Shiu et al. "Physical layer security in wireless networks: A tutorial". In: *IEEE wireless Communications* 18.2 (2011), pp. 66–74 (cit. on pp. 21–23).

[50] S. S. Manvi and S. Tangade. "A survey on authentication schemes in VANETs for secured communication". In: *Vehicular Communications* 9 (2017), pp. 19–30 (cit. on p. 21).

[51] S. Yu et al. "Achieving secure, scalable, and fine-grained data access control in cloud computing". In: *2010 Proceedings IEEE INFOCOM*. Ieee. 2010, pp. 1–9 (cit. on p. 21).

[52] A. Tchernykh et al. "Towards understanding uncertainty in cloud computing with risks of confidentiality, integrity, and availability". In: *Journal of Computational Science* 36 (2019), p. 100581 (cit. on p. 21).

[53] A. Chorti et al. "Physical layer security in wireless networks with passive and active eavesdroppers". In: *2012 IEEE Global Communications Conference (GLOBECOM)*. IEEE. 2012, pp. 4868–4873 (cit. on p. 22).

[54] G. Noubir. "On connectivity in ad hoc networks under jamming using directional antennas and mobility". In: *International Conference on Wired/Wireless Internet Communications*. Springer. 2004, pp. 186–200 (cit. on p. 22).

[55] E. McCune. "DSSS vs. FHSS narrowband interference performance issues". In: *RF Signal Processing Magazine* (2000) (cit. on p. 23).

[56] D. Abbasi-Moghadam, V. T. Vakili, and A. Falahati. "Combination of turbo coding and cryptography in NONGEO satellite communication systems". In: *2008 International Symposium on Telecommunications*. IEEE. 2008, pp. 666–670 (cit. on p. 23).

[57] J. Sherman. "Properties of focused apertures in the fresnel region". In: *IRE Transactions on Antennas and Propagation* 10.4 (1962), pp. 399–408. DOI: 10.1109/TAP.1962.1137900 (cit. on pp. 25, 26).

[58] B. Friedlander. "Localization of signals in the near-field of an antenna array". In: *IEEE Transactions on Signal Processing* 67.15 (2019), pp. 3885–3893 (cit. on pp. 25–27).

[59] P. Ramezani and E. Björnson. "Near-field beamforming and multiplexing using extremely large aperture arrays". In: *arXiv preprint arXiv:2209.03082* (2022) (cit. on pp. 26–28, 39).

[60] K. T. Selvan and R. Janaswamy. "Fraunhofer and Fresnel Distances: Unified derivation for aperture antennas". In: *IEEE Antennas and Propagation Magazine* 59.4 (2017), pp. 12–15. DOI: 10.1109/MAP.2017.2706648 (cit. on p. 28).

[61] K. T. Selvan and R. Janaswamy. "Fraunhofer and Fresnel Distances: Unified derivation for aperture antennas." In: *IEEE Antennas and Propagation Magazine* 59.4 (2017), pp. 12–15 (cit. on p. 28).

[62] A. CONSTANTINE. "Antenna Theory: A Review". In: *PROCEEDINGS OF THE IEEE* 80.1 (1992), p. 7 (cit. on p. 32).

[63] E. Björnson and L. Sanguinetti. "Power scaling laws and near-field behaviors of massive MIMO and intelligent reflecting surfaces". In: *IEEE Open Journal of the Communications Society* 1 (2020), pp. 1306–1324 (cit. on pp. 33, 42).

[64] H. T. Friis. "A note on a simple transmission formula". In: *Proceedings of the IRE* 34.5 (1946), pp. 254–256 (cit. on pp. 33, 42).

[65] A. Kay. "Near-field gain of aperture antennas". In: *IRE Transactions on Antennas and Propagation* 8.6 (1960), pp. 586–593. DOI: 10.1109/TAP.1960.1144905 (cit. on p. 38).

[66] E. Björnson, Ö. T. Demir, and L. Sanguinetti. "A primer on near-field beamforming for arrays and reconfigurable intelligent surfaces". In: *2021 55th Asilomar Conference on Signals, Systems, and Computers*. IEEE. 2021, pp. 105–112 (cit. on pp. 38, 57).

[67] W. Stutzman. "Estimating directivity and gain of antennas". In: *IEEE Antennas and Propagation Magazine* 40.4 (1998), pp. 7–11. DOI: 10.1109/74.730532 (cit. on p. 40).

[68] J. Wang et al. "Massive-MIMO MF beamforming with or without grouped STBC for ultra-reliable single-shot transmission using aged CSIT". In: *arXiv preprint arXiv:2110.00996* (2021) (cit. on p. 44).

[69] J. T. Yen. "Beamforming of sound from two-dimensional arrays using spatial matched filters". In: *The Journal of the Acoustical Society of America* 134.5 (2013), pp. 3697–3704 (cit. on p. 44).

[70] C. E. Shannon. "A mathematical theory of communication". In: *ACM SIGMOBILE mobile computing and communications review* 5.1 (2001), pp. 3–55 (cit. on p. 62).

[71] J. Barros and M. R. Rodrigues. "Secrecy capacity of wireless channels". In: *2006 IEEE international symposium on information theory*. IEEE. 2006, pp. 356–360 (cit. on p. 62).